

Introduction to SQUID Sensors for Electronics Engineers

Yongliang Wang ^{a,b*}

^a Shanghai Institute of Microsystem and Information Technology (SIMIT), Chinese Academy of Sciences (CAS), Shanghai 200050, China

^b CAS, Center for Excellence in Superconducting Electronics (CENSE), Shanghai 200050, China

*Corresponding author. Tel.: +86 02162511070; Fax: +86 02162127493.

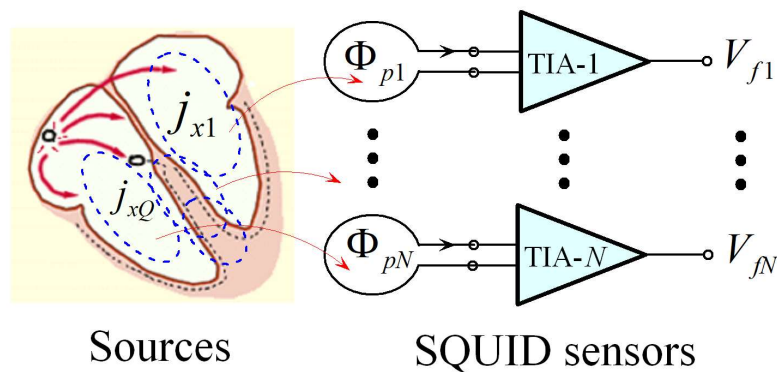
E-mail address: wangyl@mail.sim.ac.cn

ORCID: [Yong-Liang Wang \(0000-0001-7263-9493\)](https://orcid.org/0000-0001-7263-9493)

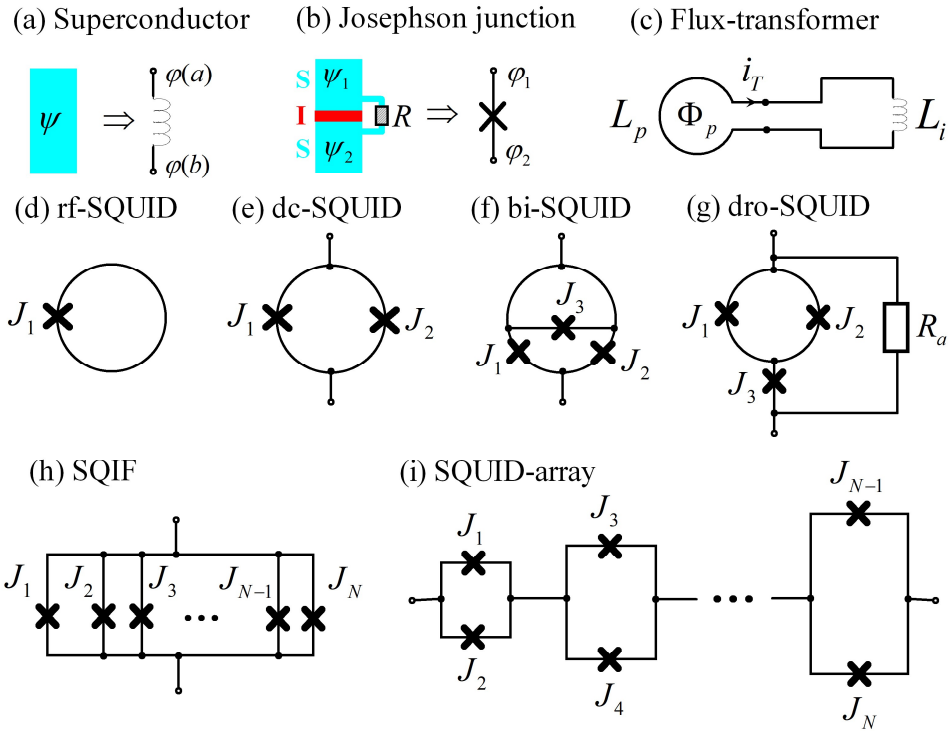
Abstract

Flux transformers and superconducting quantum interference devices (SQUIDs) are two key superconducting devices used in the cutting-edge magnetic-field sensor systems, such as magnetocardiography (MCG) and magnetoencephalography (MEG). They are superconductor integrated circuits enabled by two superconductor elements, superconductor wire and Josephson junction, based on Meissner's effect and Josephson effect. The principles of SQUID sensors are unfamiliar for electronics engineers who are trained with semiconductor electronics, due to the superconductor physics. We present an introduction to SQUID sensors, ranged from superconductor elements to the superconductor-semiconductor hybrid system. It is demonstrated that, SQUIDs inside are the resistor-inductor-capacitor (RLC) network driven by Josephson currents, and share the common network equation with normal RLC circuits; SQUID outside are magnetic-field-effect transistors (MFETs), and are dual to the semiconductor FETs in signal conversions; SQUID magnetic-field sensors are linear current amplifiers, as semiconductor FET electric-field sensors are linear voltage amplifier.

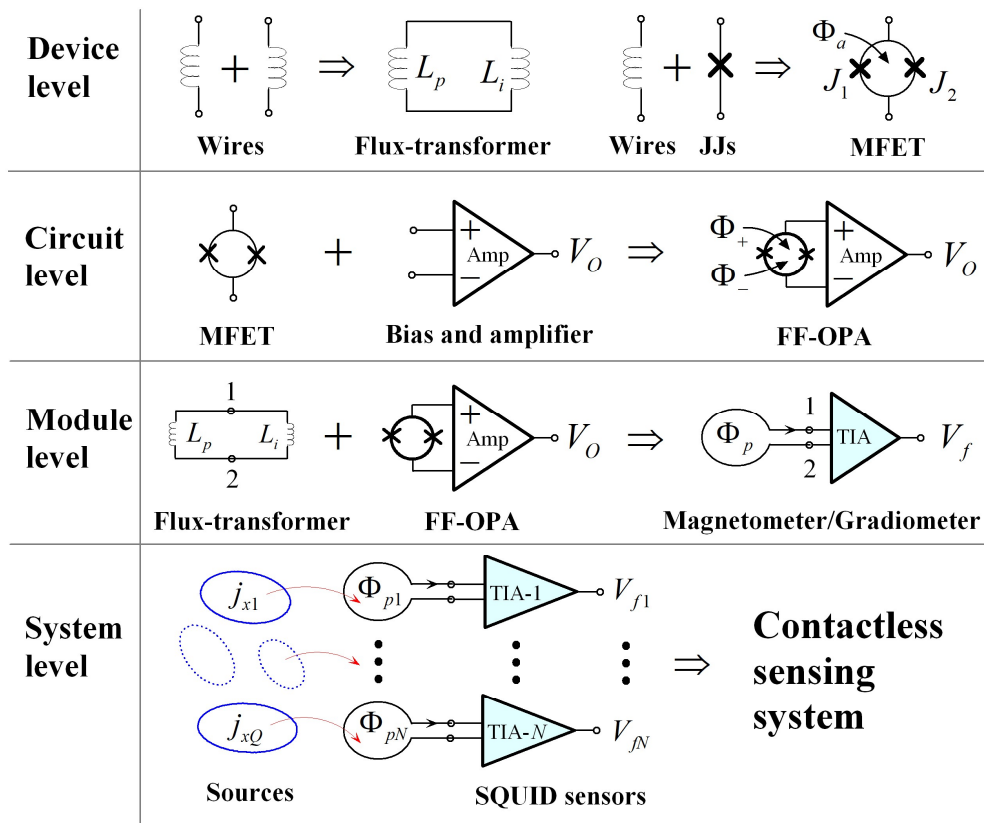
Keywords: SQUID, FF-OPA, FLL, TIA, Magnetometer, MCG, MEG.



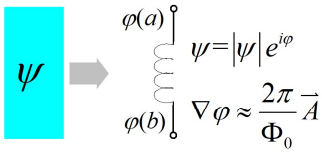
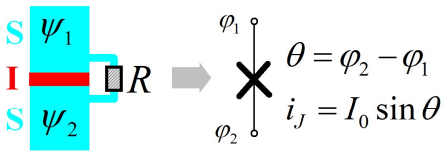
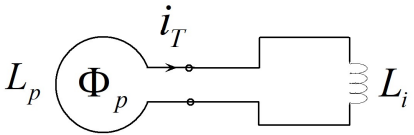
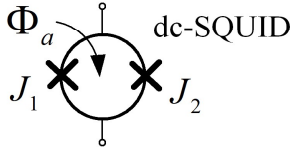
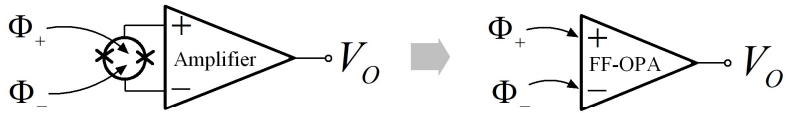
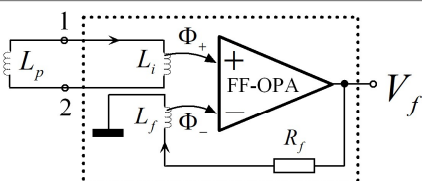
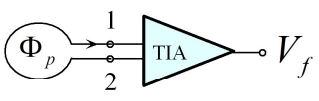
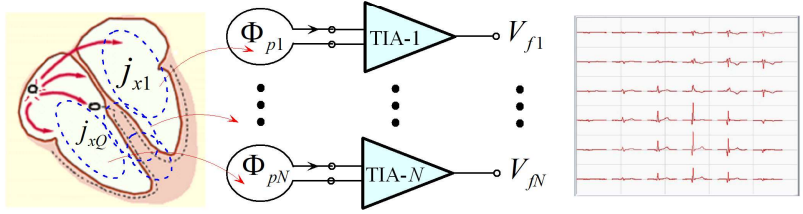
Elements and Devices



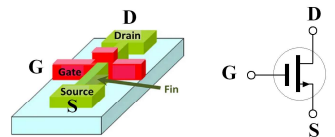
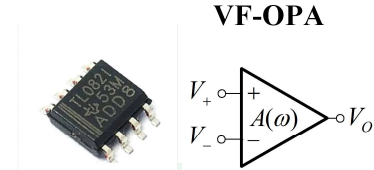
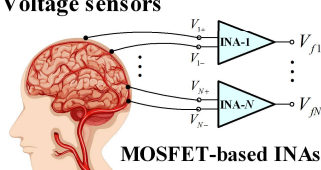
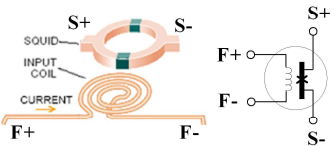
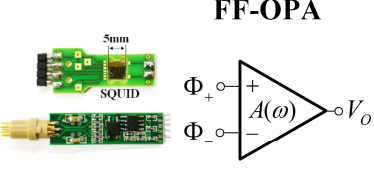
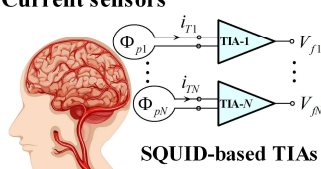
Levels of abstraction



Overview of SQUID electronics

Elements	 <p>Superconductor wire</p>	 <p>JJ: Josephson junction</p>
Devices	 <p>Flux-transformer</p>	 <p>MFET: Magnetic-field-effect transistor</p>
Flux-feedback OPA		
SQUID sensor	 <p>TIA: Trans-impedance amplifier</p>	 <p>TIA + Pickup coil : Magnetometer/Gradiometer</p>
Multi-channel SQUID system	 <p style="display: flex; justify-content: space-around;">Sources SQUID sensors Real-time signals</p>	

Duality between MOSFET and SQUID electronics

Device	Linear analog circuit	Measurement system
MOSFET 	 <p>VF-OPA</p>	Voltage sensors  <p>MOSFET-based INAs</p>
MFET 	 <p>FF-OPA</p>	Current sensors  <p>SQUID-based TIAs</p>

Abbreviations

SQUID: Superconducting Quantum Interference Device
SFQ: Single-Flux Quantum
SQIF: Superconducting Quantum Interference Filter
MCG: Magnetocardiogram
MEG: Magnetoencephalogram
FTMG: Full Tensor Magnetic Gradiometer
JJ: Josephson Junction
RLC: Resistor-Inductor-Capacitor
RCSJ: Resistively-Capacitively-Shunted Junction
FQL: Fluxoid Quantization Law
KCL: Kirchhoff's Current Law
KVL: Kirchhoff's Voltage Law
VCO: Voltage-Controlled Oscillator
MFG: Magnetic-Flux Generator
MFF: Magnetic-Flux Flow
MFET: Magnetic Field Effect Transistor
CI-MFET: Current-Input MFET
MOSFET: Metal-Oxide Semiconductor Field-Effect Transistor
AFE: Analog-Front-End
GBP: Gain-Bandwidth-Product
FLL: Flux-Locked Loop
OPA: Operational Amplifier
VF-OPA: Voltage Feedback Operational Amplifier
CF-OPA: Current Feedback Operational Amplifier
FF-OPA: Flux Feedback Operational Amplifier
INA : Instrumentation Amplifier
TIA : Trans-impedance Amplifier
CBVA : Current-Bias-Voltage-Amplifier
VBCA: Voltage-Bias-Current-Amplifier

Variables

ψ : macroscopic waver function;
 φ : macroscopic quantum phase;
 A : vector potential of magnetic field;
 Φ_0 : flux quantum; θ : phase difference;
 u : voltage difference; I_0 : critical current;
 V_s : average voltage of dc-SQUID
 ω_{rf} : resonance frequency;
 i_J : Josephson current;
 i_{cir} : SQUID loop current;
 σ_j : factor of incidence matrix;
 Φ_m : total flux in loop;

Φ_a : applied flux; i_n : noise current
 L_m : loop inductance;
 L_p : inductance of pick-up coil;
 L_i : inductance of input coil;
 n_T : number of flux quanta trapped in flux-transformer;
 Φ_p : flux picked by pick-up coil;
 I_b : external current source;
 i_b : bias current;
 i_1 : current through J_1 ;
 i_2 : current through J_2 ;
 G_{cmm} : equivalent conductance of two Josephson currents;
 V_{s0}/Φ_0 : resonance frequency
 $Z_{11}, Z_{22}, Z_{12}, Z_{21}$: network impedances;
 $A(\omega)$: open-loop gain;
 $G(\omega)$: gain of amplifier
 W_j : j -th working point;
 V_w : voltage at working point;
 n_w : number of periods;
 Φ_w : flux at working point;
 Φ_f : feedback flux
 V_n : voltage noise;
 Φ_n : flux noise;
 V_f : voltage of FLL;
 R_f : feedback resistance;
 M_f : mutual inductance of feedback coil;
 $\partial V_s/\partial \Phi_a$: flux-to-voltage transfer-coefficient;
 R_{ftr} : trans-impedance of dc-SQUID;
 V_{f_FS} : full-scale range of V_f ;
 Φ_{e_FS} : full-scale range of Φ_e ;
 R_{wire} : wire resistance;
 $SR_{\max}(f)$: maximum slew rate;
 $GBP(f)$: GBP of amplifier;
 V_m : voltage of preamplifier
 R_d : dynamic resistance of dc-SQUID;
 R_n : noise-impedance of preamplifier;
 M_I : mutual inductance for current feedback;
 M_V : mutual inductance for voltage feedback;
 R_I : impedance of current feedback;
 R_V : impedance of voltage feedback;
 Φ_{th} : threshold value of flux input;
 Φ_{in} : flux input;
 j_x : equivalent current that generates target magnetic fields;
 i_S : average value of i_{cir} ;

1. Introduction

After the discoveries of Meissner effect [1] and Josephson effect [2], various superconducting devices and circuits are developed for both analog and digital applications [3]; for example, flux transformers and superconducting quantum interference devices (SQUIDs) are devices for designing magnetic-field sensors [4], [5]; single-flux-quantum (SFQ) logics [6] are applied for power-efficient computing [7], and superconducting qubits [8] are developed for quantum computing [9]. Superconductive elements and devices [10-16] for the design of magnetic field sensors are illustrated in Fig. 1. Those devices are networks composed of resistor-inductor-capacitor (RLC) elements and two superconductor elements: superconductor wire and Josephson junction, as shown in Fig. 1(a) and (b). For instance, a flux-transformer is a closed superconducting loop of superconductor wires, as shown in Fig. 1(c); a superconducting loop inserted with one Josephson junction forms the radio-frequency (rf) SQUID, and it inserted with two Josephson junctions is called the direct-current SQUID, as shown in Fig. 1(d) and (e) respectively.

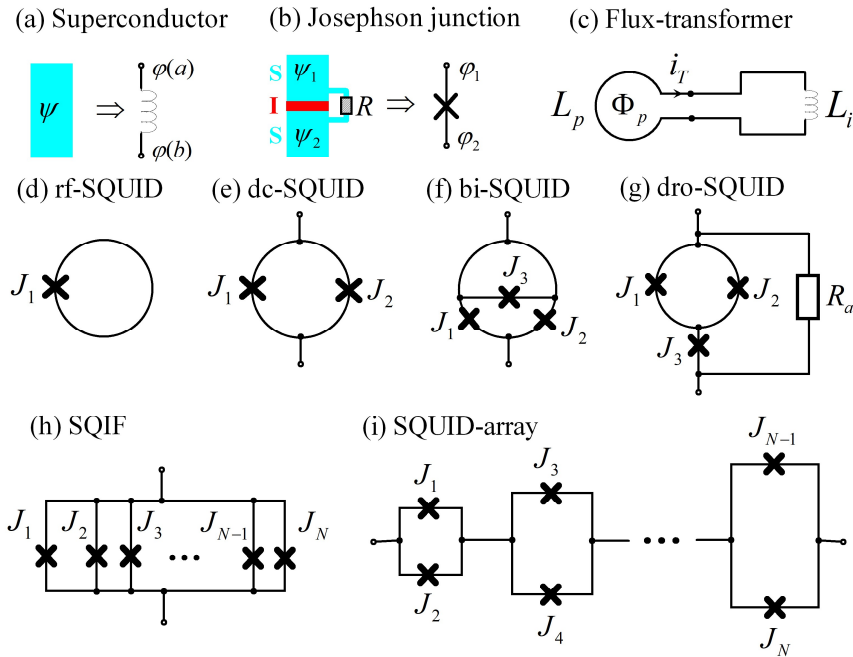


Fig. 1. Superconductor elements and devices: (a) superconductor wire; (b) resistively-shunted Josephson junction; (c) flux-transformer; (d) radio-frequency (rf) SQUID [10]; (e) dc-SQUID [11], [12]; (f) bi-SQUID [13]; (g) dro-SQUID [14]; (h) SQIF [15]; (i) SQUID-array [16].

Flux transformers are flux-to-current convertors, and SQUIDs are the most sensitive flux-to-voltage convertors; they are combined to develop many advanced magnetic field measurement systems successfully applied for biomagnetism [17], [18] and geophysical applications [19], such as magnetocardiogram (MCG), magnetoencephalogram (MEG), and full-tensor magnetic gradiometers (FTMG). In those SQUID sensors, the flux-transformer and the dc-SQUID are the flux-input front

ends for flux-to-voltage conversions, while the rest of circuits is still implemented by room-temperature semiconductor amplifiers [20]. However, electronic engineers know well the semiconductor electronics, but not the superconductor electronics, in the design of SQUID systems, for the lack of superconductor physics.

In this article, we introduce the principles of SQUID sensors in the way that can be easily understood by the electronics engineers. We interpret the basic principles of superconductor elements and derive the general network equation of superconductor integrated circuits to reveal the working mechanism inside SQUIDs; We find the general analytical expression of dc SQUIDs, and present a magnetic field-effect transistor (MFET) concept to describe the function of SQUIDs in the design of the flux- or current-based analog circuits. It is shown that SQUID-based analog circuits are dual to the analog circuits based on the metal-oxide semiconductor field-effect transistors (MOSFETs), in both the design concepts and working principles.

2. Overview of SQUID electronics

2.1 Basic concepts

The overview of SQUID electronics, ranged from basic superconductive elements to sensor system, is illustrated in Fig. 2, where the concepts and objects for the design of SQUID systems are described as follows:

- 1) **Superconductor wire**: it is a strip of superconductor, which is not only a perfect conductor, but also a magnetic field coupler. its macroscopic phase difference at two terminals records the integral of magnetic vector potentials [21].
- 2) **Resistively-shunted Josephson junction**: it is a nonlinear phase-difference creator driven by the current; its equivalent circuit is described by the so-called Resistively-capacitively-shunted junction (RCSJ) model [22].
- 3) **Flux-transformer**: it is a superconducting loop connected with pure superconductor wires, which converts the flux coupled by the loop proportionally into superconducting current circulating inside the loop [5].
- 4) **Magnetic-field-effect transistor (MFET)** [23]: it is a kind of nonlinear device which resistance is modified by the applied magnetic fields; dc-SQUID is a kind of MFET; its resistance is modulated by the flux coupled by the superconducting loop. If the flux inputs of MFETs are applied through input coils, the combination of a MFET and the input coils is the current-inputted MFET (CI-MFET).
- 5) **Flux-feedback operational amplifier (FF-OPA)** [24]: it is a kind of operational amplifier simply realized by using a MFET as the flux-input front-end before a room-temperature operational amplifiers, where the MFET is used to implement the flux-to-voltage conversion.
- 6) **Flux-locked loop** [25]: it is exactly a flux-follower implemented by the FF-OPA working in closed-loop, similar as the voltage-follower implemented by the semiconductor voltage-feedback operational amplifier (VF-OPA).
- 7) **SQUID magnetometer or gradiometer**: it is realized with a FLL tightly coupled

to a flux-transformer. constitute, depending on the style of the pick-up coil.

- 8) **Trans-impedance amplifier:** a FLL integrated with an input coil works as a SQUID-based trans-impedance amplifier (TIA) [26]. A SQUID sensor is a SQUID-based TIA connected with a pick-up coil; magnetometers and gradiometers are only different in the style of pick-up coils.
- 9) **Multi-channel SQUID system:** it is a multi-channel current-sensing system based on SQUID sensors. For example, the SQUID-based magnetocardiography (MCG) and magnetoencephalography (MEG) systems use multi-channel SQUID sensors to pick up and read out the magnetic fields generated by the target current flows; they record the real-time signals of the target magnetic fields, and finally study the target through solving the inverse problem [17].

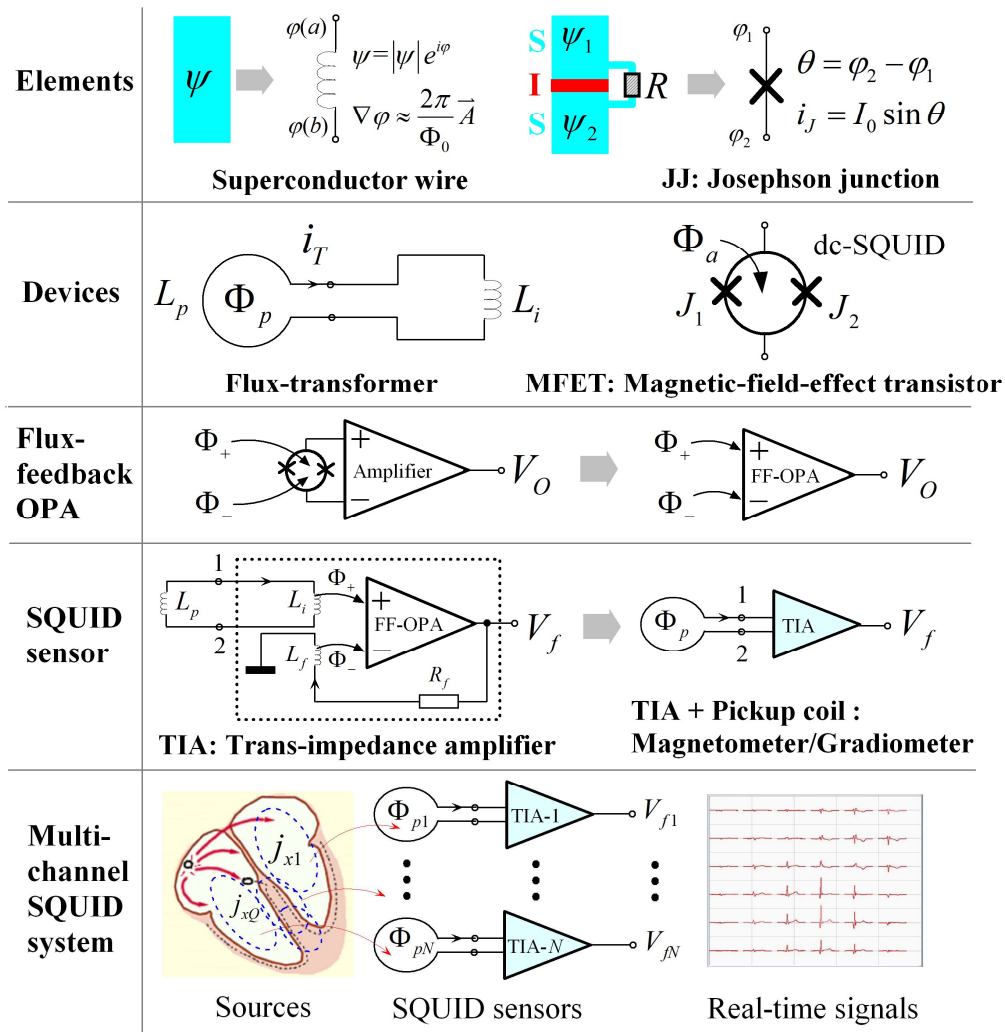


Fig. 2. Overview of SQUID-based analog circuits and systems.

The concepts of SQUID electronics above bring us an insight that, SQUID sensors are exactly the analog ‘integrated’ circuits of superconducting devices and semiconductor amplifiers, although SQUIDs and room-temperature amplifiers have to be installed separately for different working temperatures.

2.2 Levels of abstraction

There are four levels of abstraction in the design of a SQUID sensor systems, as summarized in Fig. 3:

1) At **device level**, we use two superconductor elements, superconducting wire and Josephson junction, to design flux-transformers and SQUID-based MFETs. The circuit analysis methods for resistor-inductor-capacitor (RLC) networks are also suitable for the superconducting devices, as long as we use the macroscopic quantum phases as variables to replace the voltages.

2) At **circuit level**, FF-OPAs are the analog integrated circuits of SQUID-based MFETs and room-temperature amplifiers; they use fluxes as inputs, similar to the semiconductor OPAs, in the design of analog circuits and systems.

3) At **module level**, SQUID sensors are the combination of a pick-up coil and a SQUID-based TIA; they combine the functions of the flux-transformer and the closed-loop FF-OPA.

4) At **system level**, a multi-channel SQUID system is a group of SQUID sensors configured with different pick-up coils; it is a contactless current sensing system, where, the pick-up coils sense the currents flowing inside the object under test, and linearly convert them into voltages through SQUID TIAs.

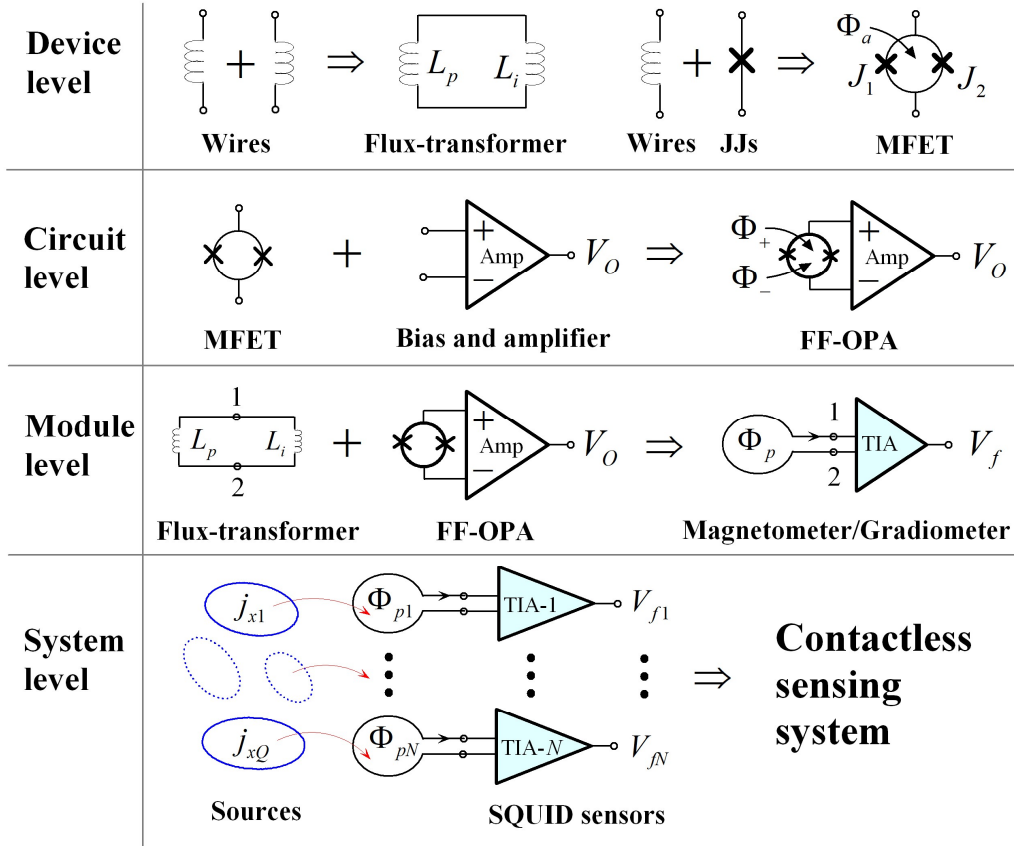


Fig. 3. Levels of abstraction for SQUID-based analog circuits and systems.

2.3 Duality between MFET and MOSFET

Fig. 4 exhibits the charge-flux duality between MFET and MOSFET electronics. MOSFETs and their application circuits and systems are electric-field or charge oriented [27], while SQUID-based MFETs and their circuits and systems are magnetic-field oriented; two devices use similar schemes in the design of analog circuits and systems.

The comparison between SQUID-based MFET and MOSFET electronics is summarized in Table 1.

Table 1. Comparison between SQUID and MOSFET electronics

	SQUID electronics	MOSFET electronics
Physics	Superconductor physics	Semiconductor physics
Circuit theory	Flux-oriented	Charge-oriented
Elements	Josephson junctions and RLC elements	PN junctions and RLC elements
Device level	Magnetic FET	Electric FET
Circuit level	Flux/current Feedback OPA	Charge/voltage Feedback OPA
Module level	Flux/current follower	Charge/voltage follower
System level	Flux/current sensing system	Charge/voltage detecting system

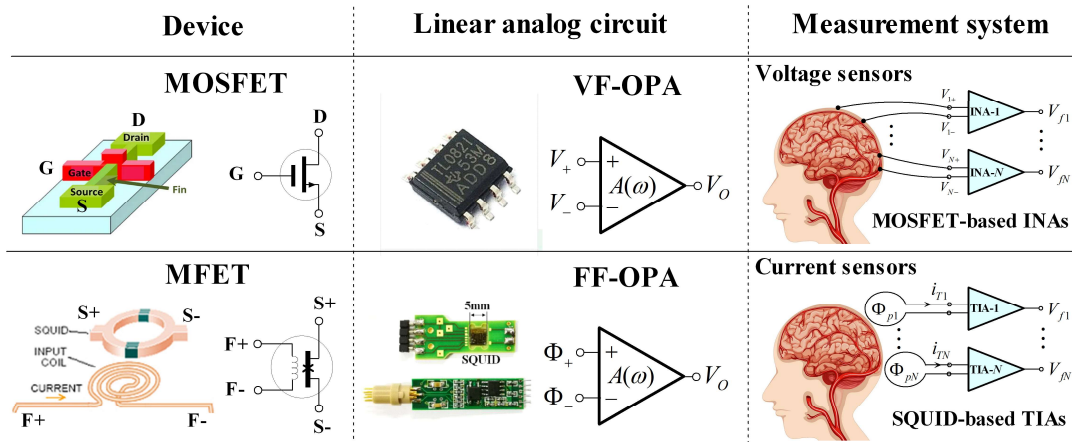


Fig. 4. Charge-flux duality between MOSFET and SQUID electronics.

2.4 Circuit theory for SQUID electronics

Four variables are used in the analysis of electric circuits [28], as shown in Fig. 5. The charge Q and flux Φ are the entities of electric and magnetic fields; their flow rates are current i and v , respectively. The principles of using circuit variables are:

- 1) Magnetic field-oriented circuits are the flux-current systems; they are usually analyzed with Φ and i as variables;
- 2) Electric field-oriented circuits are the charge-voltage systems; they are usually analyzed with Q and v as variables.

SQUIDs and their application circuits are magnetic-field oriented, and are analyzed as flux-current circuit systems. Details about circuit variables and analysis methods are

seen in the reference [29].

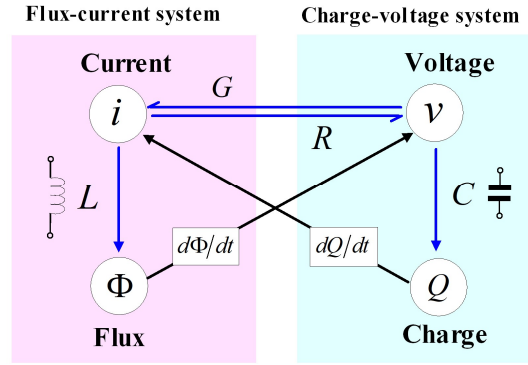


Fig. 5. Variables and elements in the electric circuit analyses.

3. Principles of superconductor elements

3.1 Superconductor elements

Superconductor circuits are superconducting RLC networks, in which superconductor wire and Josephson junction shown in Fig. 6 are the two unique elements that make superconductor circuits different from normal RLC circuits.

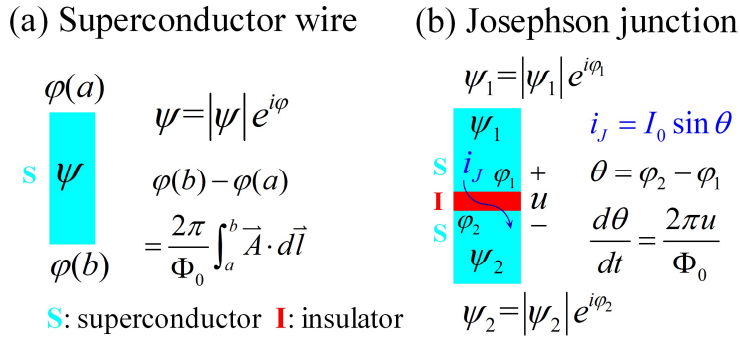


Fig. 6. Superconductor elements: (a) Superconductor wire, and (b) Josephson junction.

Superconductor wires achieve two properties:

- 1) They are the perfect conductors without resistance, similar with the wires in the conventional circuit graphs;
- 2) They are the magnetic-field couplers, which sense the magnetic field with their charge carriers [21].

Cooper pairs are the charge carriers of superconductor wires; their condense state is described by a macroscopic wave function, $\psi = |\psi| e^{i\varphi}$, as shown in Fig. 6(a). According to the Ginzburg-Landau theory [21], the quantum phase φ will vary along the wire with a gradient proportional to A ; the phase difference between terminal- a and terminal- b of superconductor wire is

$$\varphi(b) - \varphi(a) = \frac{2\pi}{\Phi_0} \int_a^b \vec{A} \cdot d\vec{l} \quad (1)$$

where Φ_0 is the flux quantum, $\Phi_0 = h/2e = 2.07 \times 10^{-15}$ Wb.

Josephson junctions have a superconductor-insulator-superconductor (SIS) structure, as illustrated in Fig. 6(b), where φ_1 is the phase at the '+' terminal and φ_2 is the one at the '-' terminal; the two-terminal phase difference is θ , and $\theta = \varphi_2 - \varphi_1$, which changes with the voltage u . Josephson current i_J is tunnelling through the insulator, which relation with the two-terminal phase and voltage is

$$\begin{cases} i_J = I_0 \sin \theta \\ \theta = \varphi_2 - \varphi_1 \\ \frac{d\theta}{dt} = \frac{2\pi u}{\Phi_0} \end{cases} \quad (2)$$

where I_0 is the critical current of the Josephson junction.

Josephson junctions implement two functions in superconducting circuits:

- 1) They are phase-difference generators, which create a phase gap between two superconductors.
- 2) Their Josephson currents are voltage-controlled oscillators (VCOs) [30-32], which are oscillating with a fundamental frequency ω_{rf} controlled by the average voltage V_s at the two terminals.

The VCO function of Josephson currents is described as follows:

$$\begin{cases} i_J = I_0 \sin \theta = I_0 \sin(\omega_{rf}t + \theta(0) + \Delta\theta) \\ \omega_{rf} = \frac{2\pi V_s}{\Phi_0}; |\Delta\theta| < C_\theta \\ V_s = \frac{1}{T} \int_0^T u \cdot dt; T \gg \frac{2\pi}{\omega_{rf}} \end{cases} \quad (3)$$

where C_θ is a bounded constant for the $\Delta\theta$, and ω_{rf} is the angular frequency controlled by the average voltage V_s , with a voltage-to-frequency ratio of 0.438 GHz/ μ V.

3.2 Closed-loop law

The closed loops connected by two kinds of superconductor elements will comply with the fluxoid quantization law (FQL) [21]. A superconducting loop connected by N Josephson junctions (N is an integer) and N superconductor is illustrated in Fig. 7, where each wire has a phase difference generated by the magnetic vector potential, and each gap between two wires has a phase difference created by the Josephson junction. Those phase differences will meet the uniqueness of the macroscopic wave function inside wires as

$$\begin{aligned} \sum_{i=1}^N (\varphi_i(a_i) - \varphi_i(b_i)) + \sum_{i=1}^N \sigma_i \theta_i &= 2n\pi \\ n \in \mathbb{Z}; \sigma_i &= \begin{cases} +1; & \text{if } i_{cir} \text{ enters '+' of } \theta_i \\ -1; & \text{if } i_{cir} \text{ enters '-' of } \theta_i \end{cases} \end{aligned} \quad (4)$$

The factor σ_i exhibits the polarity of θ_i inside the loop, with the direction of loop current i_{cir} as the reference. For instance, in Fig. 7, σ_1 is 1, since i_{cir} enters the '+' terminal of θ_1 , while σ_2 is -1, since i_{cir} enters the '-' terminal of θ_2 .

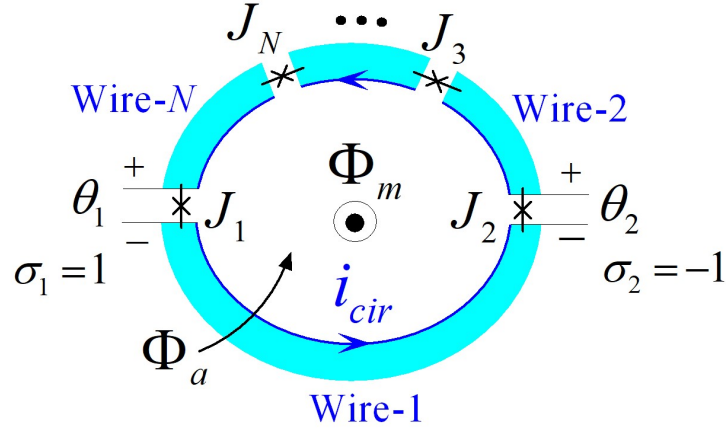


Fig. 7. Superconducting loop connected by N Josephson junctions

According to (1), we can sum the phase differences of N superconductive wires, and find that

$$\sum_{i=1}^N (\varphi_i(a_i) - \varphi_i(b_i)) = \frac{2\pi}{\Phi_0} \sum_{i=1}^N \left(\int_{a_i}^{b_i} \vec{A} \cdot d\vec{l} \right) \approx \frac{2\pi}{\Phi_0} \oint_i \vec{A} \cdot d\vec{l} = \frac{2\pi}{\Phi_0} \Phi_m \quad (5)$$

Therefore, we can derive the so-called fluxoid-quantization law (FQL) as

$$\Phi_m + \frac{\Phi_0}{2\pi} \sum_{i=1}^N \sigma_i \theta_i = n\Phi_0 \quad (6)$$

The derivative of FQL with respect to time is the Faraday's law of electromagnetic induction and the Kirchoff's voltage law (KVL):

$$\frac{d\Phi_m}{dt} + \sum_{i=1}^N \sigma_i u_i = 0 \quad (7)$$

In other words, the FQL is the integral form of the Faraday's law and KVL, in which the constant is specified as $n\Phi_0$. Therefore, the closed-loop law in (6) is general for both superconducting and normal loops.

In a loop with a self-inductance L_m , the flux Φ_m coupled by the loop is applied by the external flux Φ_a and generated by the loop current i_{cir} , thus,

$$\Phi_m = L_m i_{cir} - \Phi_a \quad (8)$$

where the self-induced flux is assumed to cancel the applied flux Φ_a .

4. Flux transformer

4.1 Principle of flux-transformer

A Flux-transformer is a superconducting loop purely connected by superconductor wires, as illustrated in Fig. 8, where there is a superconducting current, namely i_T , flowing through a pick-up coil L_p and an input coil L_i . According to the FQL, the total flux coupled in the loop must be quantized as

$$\Phi_m = n_T \Phi_0 \quad (9)$$

where, n_T is the number of flux quanta trapped in the loop.

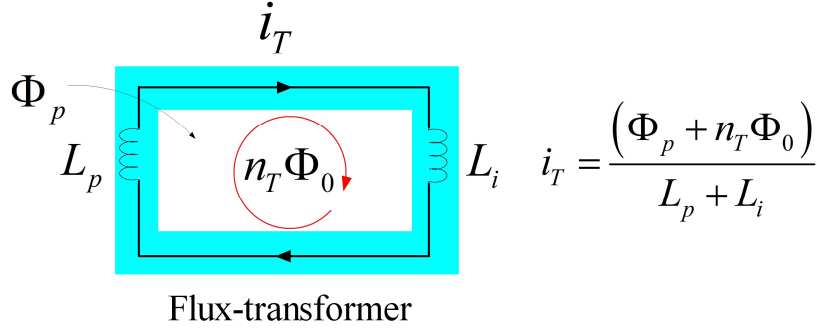


Fig. 8. Flux-transformer consists of a pick-up coil and an input coil.

The flux-transformer will turn the flux Φ_p picked-up by the pick-up coil linearly into loop current i_T ; the function of i_T will be calculated by Φ_p as

$$\Phi_m = (L_p + L_i) i_T - \Phi_p \Rightarrow i_T = \frac{\Phi_p + n_T \Phi_0}{L_p + L_i} \quad (10)$$

Accordingly, flux transformers are linear flux-to-current convertors.

4.2 Styles of pick-up coils

Pick-up coils have various styles to extract the components of magnetic fields [4], [5], as illustrated in Fig. 9. The pick-up coil for magnetometers is winding along a planar surface, as shown in Fig. 9(a); the first-order gradiometer has two planar surfaces, as shown in Fig. 9(b); the second-order gradiometer have four planar surfaces, as exhibited in Fig. 9(c). The flexible configuration of pick-up coils for different targets is one of the advantages of SQUID sensors.

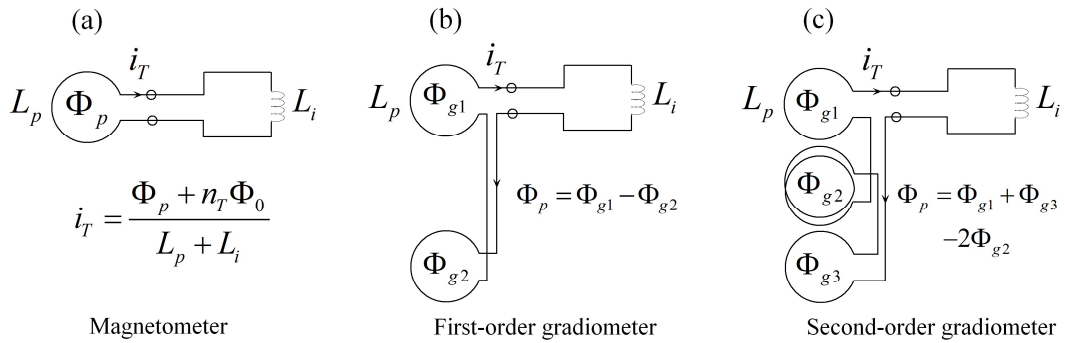


Fig. 9. Flux transformers: (a) pick-up coil is a magnetometer; (b) pick-up coil is a first-order gradiometer; (c) pick-up coil is a second-order gradiometer.

5. Magnetic field-effect transistor

5.1 Structure of dc-SQUID

A dc-SQUID is a superconducting loop inserted with two Josephson junctions, as shown in Fig. 10(a), where two terminals of Josephson junctions are led to a bias current source I_b , and a non-zero average voltage V_s will be measured when the bias current is

larger than the critical current of Josephson junctions. The equivalent circuit of the dc-SQUID is a RLC network driven by two Josephson currents, as shown Fig. 10(b), where i_{n1} and i_{n2} are noise currents. Each Josephson junction is treated as a RCSJ [22], and is symbolized as shown in Fig. 10(c); accordingly, the dc-SQUID is represented with a two-terminal device as shown in Fig. 10(d).

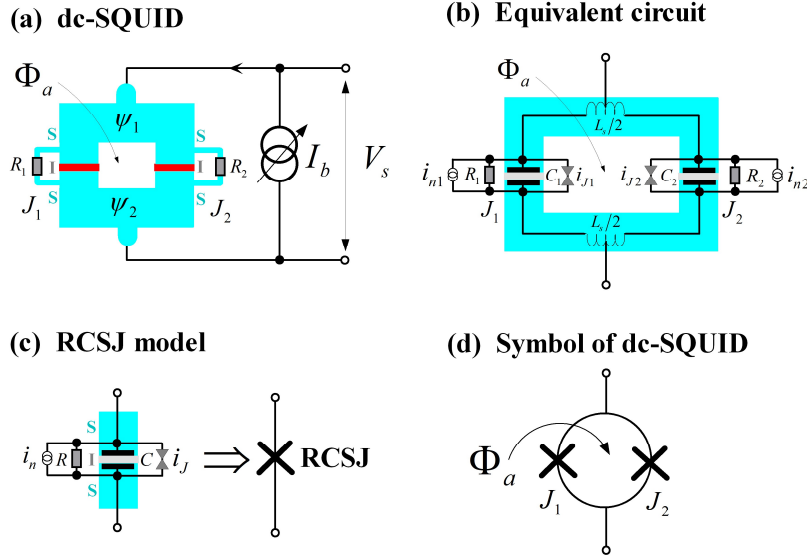


Fig. 10. (a) dc-SQUID under current bias. (b) Equivalent circuit of dc-SQUID. (c) RCSJ model. (d) Symbol of dc-SQUID

5.2 Circuit equations of dc-SQUID

The dc-SQUID loop contains a superconducting current i_{cir} , as defined in Fig. 11(a). The i_1 and i_2 flowing through two Josephson junctions are supplied by the i_{cir} and bias current I_b ; therefore, the dc-SQUID can be redrawn as shown in Fig. 11(b), where each Josephson junction is separately biased with $I_b/2$.

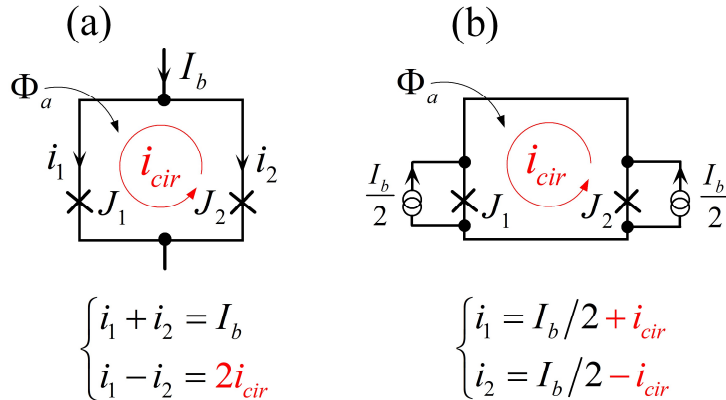


Fig. 11. (a) Superconducting current circulating in dc-SQUID loop. (b) Equivalent circuit of dc-SQUID, where two Josephson junctions are separately biased.

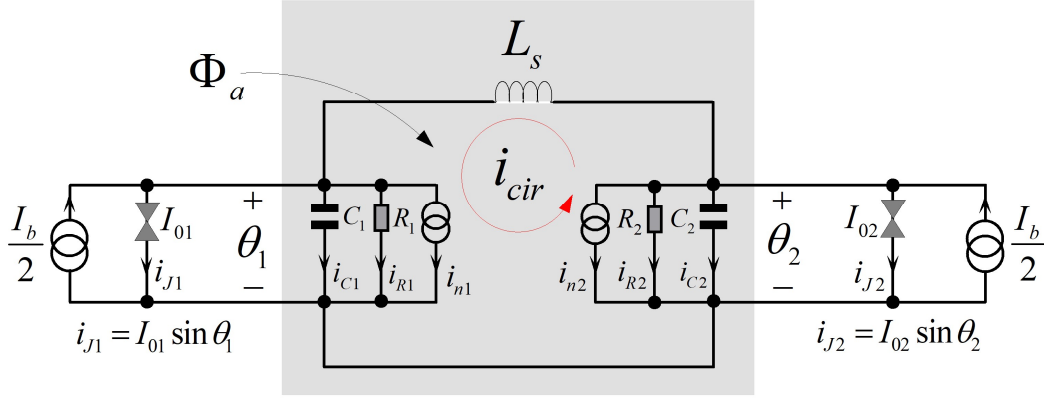


Fig. 12. Two-port dc-SQUID network driven by Josephson currents [23].

The dc-SQUID is equivalent to a two-port network equivalent circuit [23], as shown in Fig. 12. The two-port RLC network is driven by two Josephson currents and two bias currents. Josephson currents, i_{J1} and i_{J2} , are the phase-controlled current sources; the I_b and Φ_a are the given inputs, while the θ_1 and θ_2 are two outputs. The circuit equations of the dc-SQUID are derived as follows:

First, the FQL in the SQUID loop is written as

$$L_s i_{cir} - \Phi_a + \frac{\Phi_0}{2\pi} (\theta_1 - \theta_2) = 0 \quad (11)$$

Second, two current-phase relations of Josephson junctions are

$$\begin{cases} \frac{\Phi_0 C_1}{2\pi} \theta_1' + \frac{\Phi_0}{2\pi R_1} \theta_1 + I_{01} \sin \theta_1 + i_{n1} = \frac{I_b}{2} + i_{cir} \\ \frac{\Phi_0 C_2}{2\pi} \theta_2' + \frac{\Phi_0}{2\pi R_2} \theta_2 + I_{02} \sin \theta_2 + i_{n2} = \frac{I_b}{2} - i_{cir} \\ \theta_1' = \frac{d^2 \theta_1}{dt^2}; \theta_2' = \frac{d^2 \theta_2}{dt^2}; \theta_1 = \frac{d\theta_1}{dt}; \theta_2 = \frac{d\theta_2}{dt} \end{cases} \quad (12)$$

5.3 Dynamics inside dc-SQUID

The circuit equations of dc-SQUID in (11) and (12) are exhibited by a system diagram shown in Fig. 13 [33]. The module colored in grey is a second-order linear system modified by two nonlinear phase-to-current feedback functions, i_{J1} and i_{J2} . The dynamics of this system are described as follows:

- 1) In zero-voltage state, θ_1 and θ_2 are stable in a certain value that enable i_{J1} and i_{J2} to cancel the i_1 and i_2 supplied by I_b and i_{cir} .
- 2) In voltage state, θ_1 and θ_2 will keep increasing because i_{J1} and i_{J2} are less than i_1 and i_2 ; the average increasing speed of θ_1 and θ_2 is proportional to the measured voltage V_s of dc-SQUID.
- 3) The external Φ_a is turned into i_{cir} to adjust the bias currents of two Josephson junctions, and thereby modulates the average speed of θ_1 and θ_2 ; this is how the flux-modulated current-voltage characteristics of dc-SQUID are formed.

Therefore, under the same average voltage V_s , two Josephson currents are working as two VCOs, and are driving the two-port RLC network in oscillation state; the fundamental oscillation frequency ω_{rf} is defined in (3).

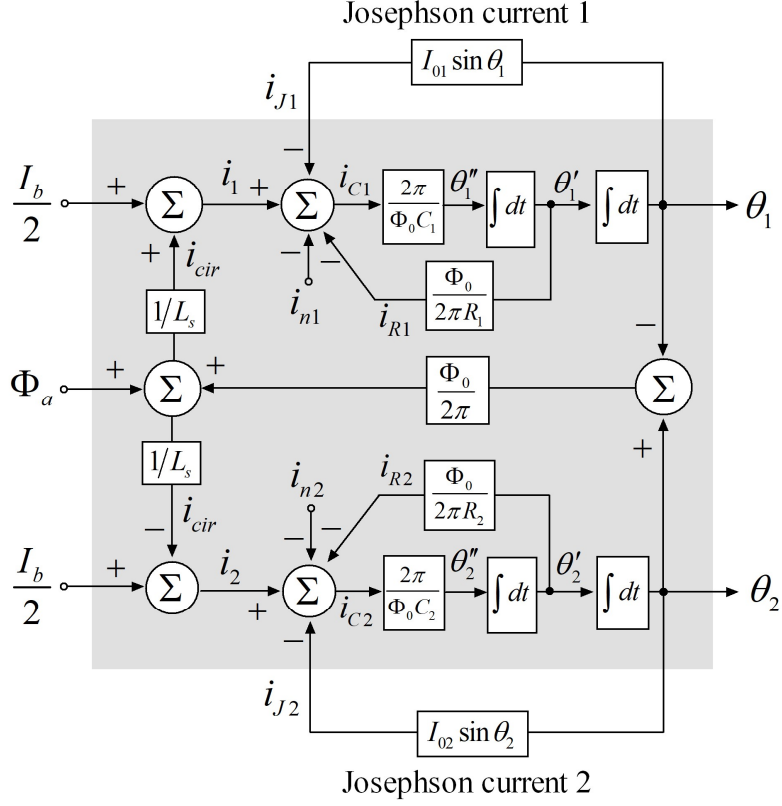


Fig. 13. System diagram of dc-SQUID [33].

5.4 Magnetic-flux-flow diagram of dc-SQUID

SQUIDs and single-flux-quantum (SFQ) gates, as well as Josephson qubits, are all the superconducting RLC networks driven by additional Josephson currents, and are unified with normal RLC circuits with a common network equation [34], [35]. The general network equation in matrix is

$$\begin{aligned} \mathbf{C} \frac{d^2 \Phi_{EL}}{dt^2} + \mathbf{G} \frac{d \Phi_{EL}}{dt} + \mathbf{I}_0 \sin \left(\frac{2\pi \Phi_{EL}}{\Phi_0} \right) + \sigma^T \mathbf{L}_m^{-1} \sigma \Phi_{EL} \\ = \mathbf{i}_b - \mathbf{i}_n + \sigma^T \mathbf{L}_m^{-1} (\mathbf{Const} + \Phi_a) \end{aligned} \quad (13)$$

The variable vectors and parameter matrices for the dc-SQUID shown in Fig. 12 are

$$\begin{cases} \Phi_{EL} = [\Phi_{EL1} \quad \Phi_{EL2}]^T = \frac{\Phi_0}{2\pi} [\theta_1 \quad \theta_2]^T; \mathbf{Const} + \Phi_a = [\Phi_a] \\ \mathbf{i}_b = \left[\frac{I_b}{2} \quad \frac{I_b}{2} \right]^T; \mathbf{i}_n = [i_{n1} \quad i_{n2}]^T; \sigma = [1 \quad -1]; \mathbf{L}_m = [L_s] \\ \mathbf{C} = \begin{bmatrix} C_1 & 0 \\ 0 & C_2 \end{bmatrix}; \mathbf{G} = \begin{bmatrix} 1/R_1 & 0 \\ 0 & 1/R_2 \end{bmatrix}; \mathbf{I}_0 = \begin{bmatrix} I_{01} & 0 \\ 0 & I_{02} \end{bmatrix} \end{cases} \quad (14)$$

This general network equation is derived by a genal flux-based circuit theory [36]. In this theory, Josephson junction circuits can be described with a general network equation and simulated with a general system model; they can also be redrawn with magnetic-flux-flow (MFF) diagrams [35] to vividly depict flux-flow dynamics.

For example, the dc-SQUID shown in Fig. 14(a) is further exhibited with a magnetic-flux-flow diagram, as shown in Fig. 14(b). This MFF diagram reveals the flux-flow mechanism inside dc-SQUID as follows:

- 1) Two current-biased Josephson junctions are two magnetic-flux generators (MFGs), namely MFG-1 and MFG-2. In the conventional circuit diagram, two Josephson junctions are inserted in the SQUID loop, Loop-1, while they are connected to Loop-1 in the MFF diagram;
- 2) MFG-2 keep pumping flux quanta into Loop-1, while MFG-1 keep drawing the flux quanta out of Loop-1. The average flow-rate of the flux flow pumping in and out Loop-1, is exactly the average voltage V_s that is measured at two terminals of MFG-1 and MFG-2.
- 3) The external flux Φ_a applied to Loo-1 is turned into an offset current applied to two Josephson junctions, according to (13); it will therefore alter the flow-rate, like a water-tap.

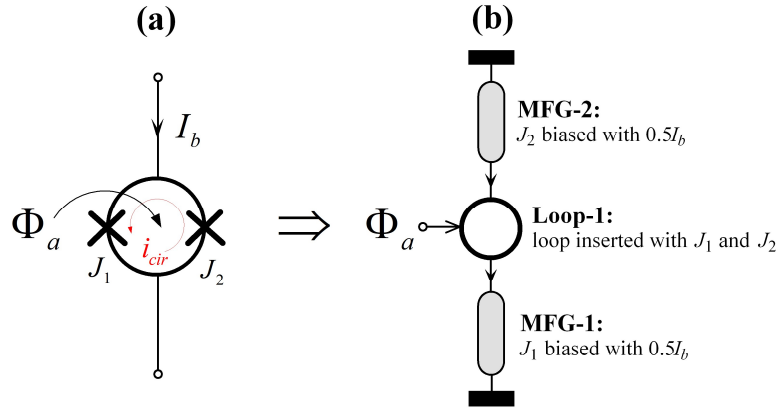


Fig. 14. (a) dc-SQUID and (b) its magnetic-flux-flow (MFF) diagram [36].

This MFF diagram vividly depicts the flux-flow dynamics inside dc SQUIDs working as MFETs. More details are seen in [35] [36].

5.5 Characteristics of dc-SQUID

The current-voltage characteristics of dc-SQUID are illustrated in Fig. 15. They are captured by measuring V_s under various Φ_a and i_b , from the dc-SQUID shown in Fig. 15(a); They can also be numerically simulated with either the system model shown in Fig. 13 or the circuit equation in (13). The measured characteristics can be well agreed by the simulations [35], if the circuit model and parameters are properly set.

With V_s and i_b as the coordinates, the current-voltage curves under different Φ_a are shown in Fig. 15(b). Those curves are expressed with a function as

$$V_s = f(i_b, \Phi_a) = f(i_b, \Phi_a + n\Phi_0); n \in \mathbb{Z} \quad (15)$$

It is a periodical function for the flux input Φ_a , in which, the period is $1\Phi_0$. By setting i_b as I_b , we can observe a periodical flux-voltage characteristic, as illustrated in Fig. 15(c); this flux-voltage curve is defined with a function as

$$V_s = f_{V-\Phi}(\Phi_a) = f(I_b, \Phi_a) \quad (16)$$

Those functions achieve practical physical meanings, in the system model shown in Fig. 13 and the MFF diagram shown in Fig. 14. In the system model in Fig. 13, those functions describe how the average increasing speed of θ_1 and θ_2 is modulated by i_b and Φ_a ; they also describe how the i_b and Φ_a tune the average flow rate of the flux flow in MFG1 and MFG2, in the MFF diagram shown in Fig. 14.

In the current-voltage curves shown in Fig. 15(b), there is a LC-resonance point, at which the flux-modulation characteristic disappears; the voltage V_{s0} indicates the resonance frequency, and can be analytically expressed with the RLC parameters inside the SQUID washer [33]. How the resonance frequency V_s under the given i_b and Φ_a is decided by circuit parameters inside the dc-SQUID can be explained by the analytical expression of the current-voltage function defined in (15).

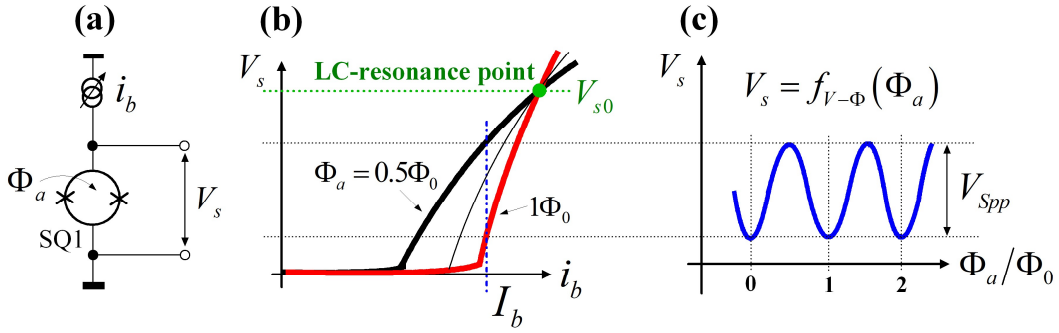


Fig. 15. Dc-SQUID and characteristics: (a) dc-SQUID under current bias; (b) flux-modulated current-voltage curves of dc-SQUID; (c) periodical flux-voltage curve of dc-SQUID.

5.6 Analytical expression of dc-SQUID

The analytical expression of (15) is difficult to be directly solved from the differential circuit equations that are varied with the equivalent circuit of dc SQUIDS [37-40]; it is still lacked in the long history of dc SQUIDS.

We proposed a general analytical expression of dc SQUIDS [23], in another form of

$$F(V_s, i_b, \Phi_a) = 0 \Rightarrow \begin{cases} i_b = f_i(V_s, \Delta\theta_{dc}) = \left(\frac{1}{Z_{11}(0)} + G_{cmm} \right) \cdot V_s \\ \Phi_a = f_\Phi(V_s, \Delta\theta_{dc}) = \frac{\Phi_0}{2\pi} \cdot \Delta\theta_{dc} + \Phi_{cir} + \eta L_s^* V_s + \alpha L_s^* i_b \end{cases} \quad (17)$$

where i_b and Φ_a are the dependent variables of the resonance frequency V_s and the average phase difference between θ_1 and θ_2 , namely $\Delta\theta_{dc}$.

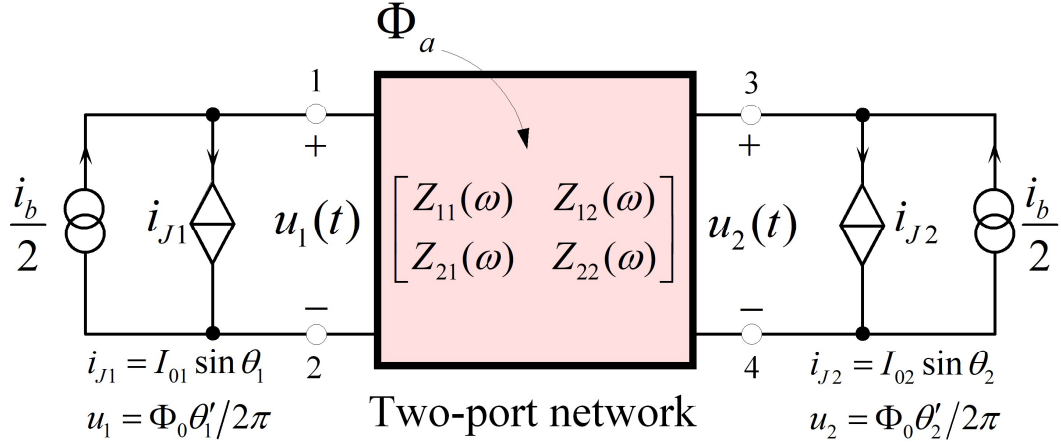


Fig. 16. A general two-port network model for dc SQUIDs [23].

This general analytical expression is derived by using a general two-port network model of dc SQUIDs, as shown in Fig. 16. The model treats any dc-SQUID circuit as a two-port network driven by the i_b and two Josephson currents. This two-port network achieve flux-modulated current-voltage characteristics, based on two principles:

- 1) Under a nonzero voltage V_s , two Josephson currents are VCOs, they generate both dc and ac currents into two-port network; the dc component of Josephson currents is proportional to the total power transferred by the ac components, due to the zero-power consumption principle of Josephson currents.
- 2) In response to i_b and two Josephson currents, the two-port network creates both the V_s and ac voltages at two ports. In frequency domain, the two-port network implements its transfer-function with only four network impedances, such as Z_{11} , Z_{22} , Z_{12} , and Z_{21} ($Z_{12} = Z_{21}$ for reciprocity principle).

The G_{cmm} in (17) is the equivalent conductance of the dc component of two Josephson currents, we find the analytical expressions of G_{cmm} with frequency domain analyses in [23]. Based on the expression of G_{cmm} , a dc-SQUID is equivalent to a flux-controlled nonlinear resistor in parallel with the $Z_{11}(0)$, as illustrated in Fig. 17.

- 1) A bare-washer dc-SQUID shown in Fig. 17(a) is equivalent to two resistors in parallel, as shown in Fig. 17(b).
- 2) A dc-SQUID coupled with one input coil and the equivalent circuit are exhibited in Fig. 17(c) and (d), where Z_{i1} is the impedance at the terminals of the input coil, and is involved in four impedances, since the input coil is a part of the two-port network.
- 3) A dc-SQUID coupled with two input coils is modeled as shown in Fig. 17(e) and (f), where both Z_{i1} and Z_{i2} will affect the impedances of the two-port network, and thereby modify the current-voltage characteristics [41-44].

Details of the derivation of G_{cmm} are seen in the reference [23]; it is shown that the G_{cmm} is the projection of the network impedances, and the real-part of impedance Z_{12} , $\text{Re}(Z_{12})$, decides the flux-modulation depth of current-voltage characteristics; the reason why there will be the crossing of current-voltage curves in Fig. 15(b) is that the

real-part of Z_{12} is zero at the LC-resonance point.

Accordingly, for a symmetric bare-washer dc-SQUID, we can derive that the V_{s0} at the LC-resonance point is decided by the loop inductance and the capacitance of one Josephson junction [33], namely

$$\frac{V_{s0}}{\Phi_0} = \frac{1}{2\pi\sqrt{L_s C_j}}; C_j = C_1 = C_2 \quad (18)$$

To be notice that, V_{s0}/Φ_0 is not the resonance frequency of the SQUID loop composed of two junction capacitances which resonance frequency is $1/\pi\sqrt{(2L_s C_j)}$. More details are seen in [23] [33].

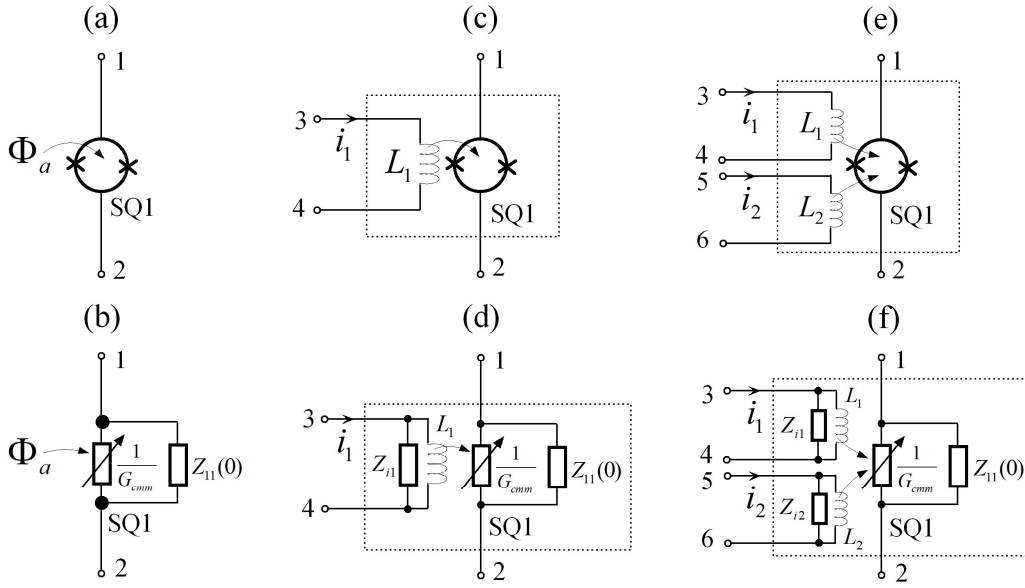


Fig. 17. Nonlinear resistance of SQUID-based MFET [23]: (a) bare-washer dc-SQUID, and (b) its nonlinear resistor model; (c) CI-MFET with one input coil, and (d) the equivalent circuit; (e) CI-MFET with two input coils, and (f) the equivalent circuit.

The general analytical expression of dc-SQUID in (17) will have two practical applications:

- 1) It can be used to characterize circuit parameters of a dc-SQUID with the measured current-voltage characteristics.
- 2) It can be used to predict the current-voltage characteristics of a dc-SQUID with the network impedances extracted from the circuit layout.

6. Flux-feedback operational amplifier

6.1 Concept of FF-OPA

Operational amplifiers (OPAs) are the general scheme to design linear analog circuits using nonlinear devices [45]. The voltage-feedback OPA (VF-OPA) and the flux-feedback OPA (FF-OPA) are illustrated in Fig. 18. With a three-terminal VF-OPA shown in Fig. 18(a), which open-loop-gain $A(\omega)$ far larger than 1, $A(\omega) \gg 1$, a linear

voltage follower is implemented by feeding the voltage output back to the inverting voltage input, as shown in Fig. 18(b). Similarly, with a three-terminal FF-OPA shown in Fig. 18(c), a linear flux-follower is realized by feeding the voltage output to the inverting flux input through a circuit consisting of a resistor and a feedback coil in serial, as illustrated in Fig. 18(d).

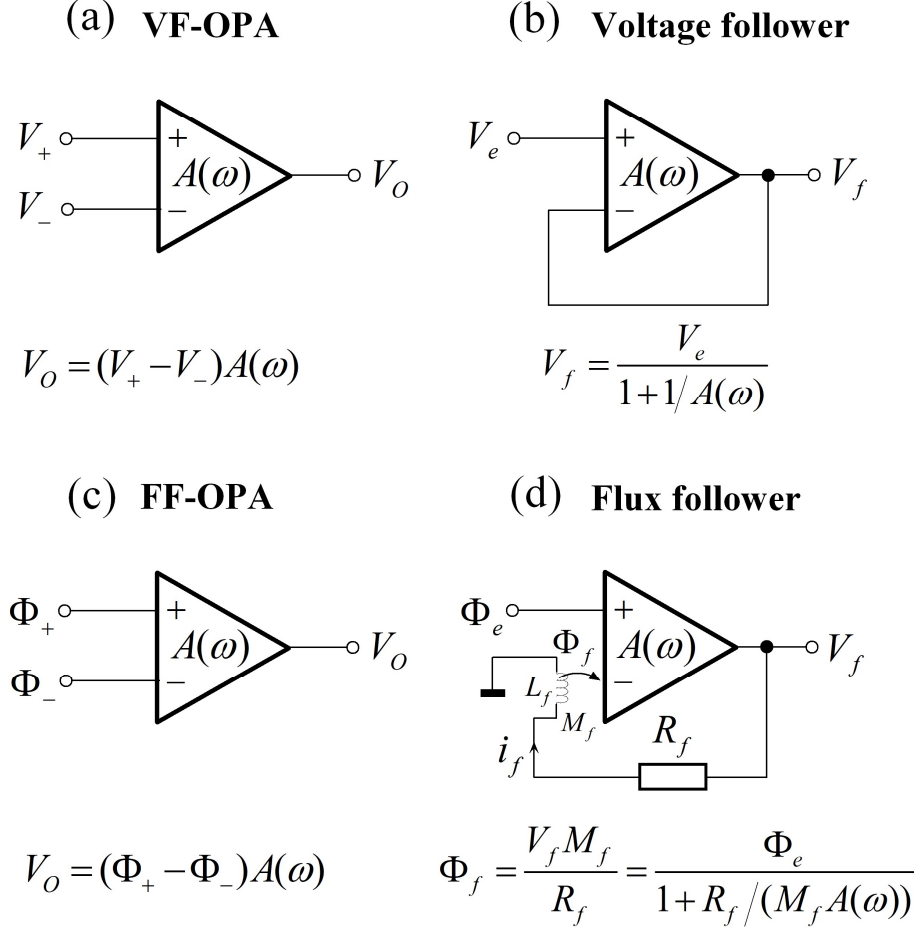


Fig. 18. (a) Voltage-feedback operational amplifier (VF-OPA) and its (b) voltage-follower circuit; (c) Flux-feedback operational amplifier (FF-OPA) and (d) its flux-follower circuit.

6.2 SQUID-based FF-OPA

A simple SQUID-based FF-OPA is shown in Fig. 19(a), where the dc-SQUID is simply a MFET used to sense the positive and negative flux inputs. The dc-SQUID is biased with a current source I_b and connected to the non-inverting input of the room-temperature amplifier U1. The current source I_r is applied on a resistor R_r to generate a voltage at the inverting input of U1.

The flux-follower based on the negative feedback mechanism is accordingly implemented with the SQUID-based FF-OPA, as shown in Fig. 19(b). It is exactly the well-known flux-locked loop (FLL), which generates Φ_f to cancel the flux input Φ_e and keep the difference between V_+ and V_- being zero, $V_+ = V_-$.

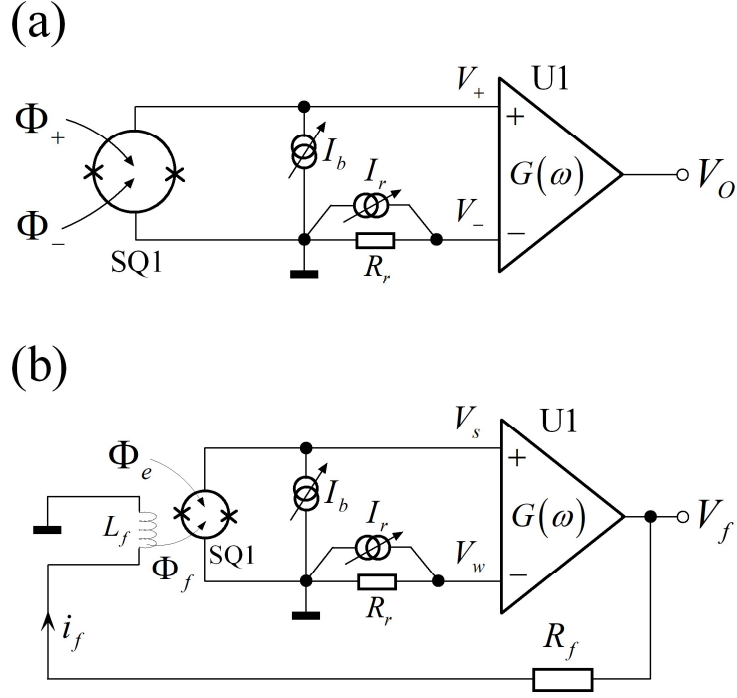


Fig. 19. (a) SQUID-based FF-OPA, (b) FLL implemented by a flux-follower [24].

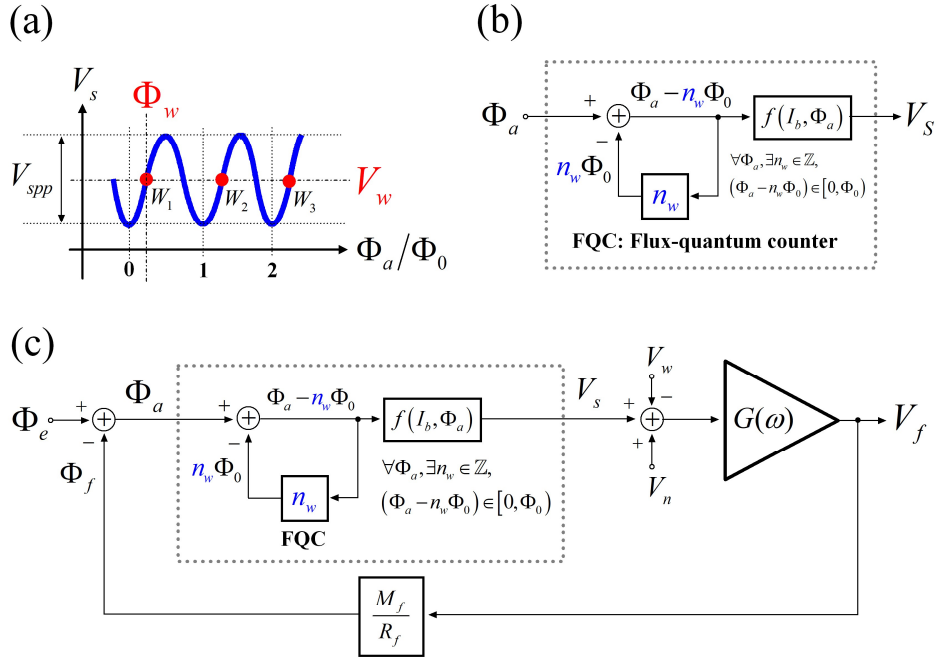


Fig. 20. (a) flux-voltage characteristic of dc-SQUID; (b) transfer function of dc-SQUID; (c) transfer function diagram of SQUID-based FLL [26].

Assuming that the input impedances of the U1 are far larger than the SQUID and R_r , and are ignorable, $V_+ = V_s$, $V_- = V_w$ and $V_w = I_r R_r$; the SQUID output V_s will be locked at V_w dynamically. The points, such as, W_1 , W_2 , and W_3 , are the working points of the FLL periodically located in the positive slopes of the current-voltage characteristic, as

illustrated in Fig. 20 (a). Since the j -th working point W_j is located at $(V_w, \Phi_w + n_w\Phi_0)$, $n_w = j - 1$; those working points are defined as

$$V_w = f(I_b, \Phi_w + n_w\Phi_0); \Phi_w \in [0, \Phi_0) \quad (19)$$

This n_w records the period where the working point is located, with which the flux-voltage function in (16) can be rewritten as

$$V_s = f_{V-\Phi}(\Phi_a - n_w\Phi_0); (\Phi_a - n_w\Phi_0) \in [0, \Phi_0) \quad (20)$$

The transfer function of this dc-SQUID is modeled as shown in Fig. 20(b), where the n_w is automatically truncated by a virtual flux-quantum counter (FQC). The SQUID-based FLL is accordingly a feedback system model, as shown in Fig. 20(c).

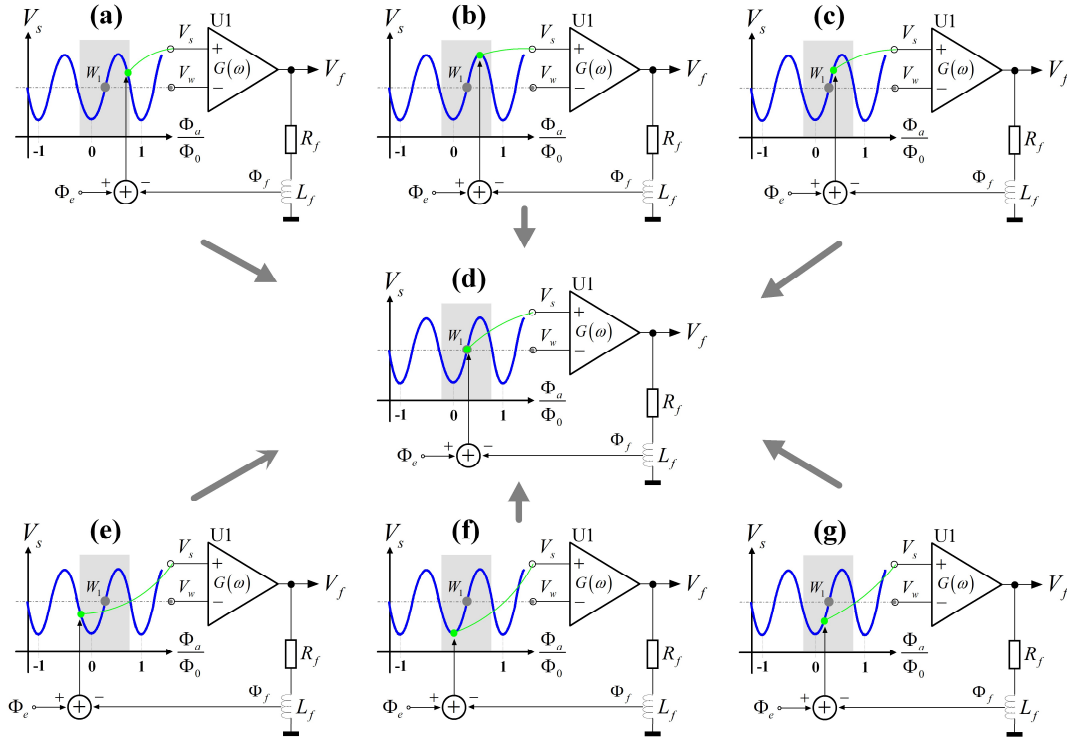


Fig. 21. Dynamic responses of dc-SQUID FLL; in the flux-voltage curve, $W_1 (V_w, \Phi_w)$ is the working point, and the point (V_s, Φ_a) is the current state of dc-SQUID: (a) the initial state (V_s, Φ_a) of dc-SQUID is at the negative slope, and $V_s > V_w$; (b) the initial state (V_s, Φ_a) is at the positive peak; (c) the initial state (V_s, Φ_a) is at the positive slope, and $V_s > V_w$; (d) the initial state (V_s, Φ_a) is coincide with W_1 ; (e) the initial state (V_s, Φ_a) is at the negative slope, and $V_s < V_w$; (f) the initial state (V_s, Φ_a) is at the negative peak; (g) the initial state (V_s, Φ_a) is at the positive slope, and $V_s < V_w$.

The responses of FLL to different initial states of Φ_a are illustrated in Fig. 21, where the dc-SQUID is depicted by its flux-voltage curve in Φ_a and V_s coordinates. The increase of Φ_e will push Φ_a to right, while the increase of Φ_f will push Φ_a to left; the output V_s is amplified by the non-inverting input of U1 with gain $G(\omega)$; it will increase V_f and Φ_f , if $V_s > V_w$, while decrease V_f and Φ_f , if $V_s < V_w$. The working principle of this system is simply described as followings:

- 1) If $V_s > V_w$, the room-temperature amplifier will increase V_f and Φ_f to push Φ_a

back to left, as shown in Fig. 21(a), (b) and (c).

- 2) If $V_s < V_w$, the room-temperature amplifier will decrease V_f and Φ_f to pull Φ_a back to right; as shown in Fig. 21(e), (f) and (g).
- 3) If $V_s = V_w$, the room-temperature amplifier will keep Φ_a stable at Φ_w , as illustrated in Fig. 21(d).

As long as the initial state (V_s, Φ_a) is within the gray area around W_1 shown in Fig. 21, the FLL will always move the Φ_a back to Φ_w . In other words, the FLL will be relocked at $\Phi_w + n_w\Phi_0$, when the initial Φ_a is in the gray area around $\Phi_w + n_w\Phi_0$.

In Fig. 21, the various initial states of Φ_a are set by the sudden change of Φ_e ; the relocking of FLL exhibits the step-response of FLL to the step input of Φ_e . The response time of FLL depends on the deflection of Φ_a :

- 1) The response time is approximately linear to the deviation of Φ_a , if the state (V_s, Φ_a) is located at the positive slope, as shown in Fig. 21(b), (c), (f) and (g).
- 2) The response time is nonlinear to the deviation of Φ_a , if the state (V_s, Φ_a) is located at the negative slope, as shown in Fig. 21(a) and (e).

In summary, a SQUID-based FLL is a flux-follower implemented by a SQUID-based FF-OPA. In the FF-OPA, the dc-SQUID is an AFE with a periodical nonlinear flux-to-voltage characteristic to sense flux inputs. The SQUID-based flux-follower is similar with the semiconductor FET-based voltage followers, except that the SQUID-based analog-front-end (AFE) has multiple working points in its flux-to-voltage characteristic while the FET-based AFE usually has only one working point.

6.3 Transfer function of FLL

In the flux-voltage characteristic shown in Fig. 22 (a), the transfer function of dc-SQUID in response to the small signal input around W_1 , is approximately defined with the transfer coefficient $\partial V_s/\partial\Phi_a$ at W_1 ; the $\partial V_s/\partial\Phi_a$ at working points is defined by the flux-voltage function as

$$\frac{\partial V_s}{\partial\Phi_a} = \left. \frac{\partial f(i_b, \Phi_a)}{\partial\Phi_a} \right|_{\substack{i_b=I_b \\ \Phi_a=\Phi_w+n_w\Phi_0}} \quad (21)$$

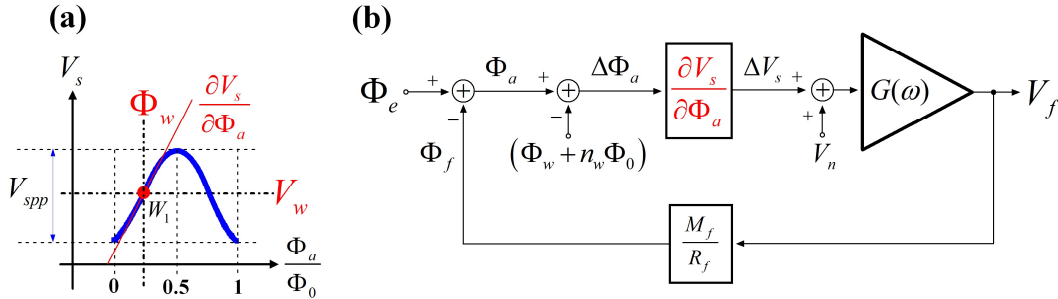


Fig. 22. (a) Transfer coefficient at W_1 ; (b) system diagram of FLL locked at W_1 [26].

With this small signal transfer function, the linear transfer function diagram of the FLL is shown in Fig. 22(b). In this model, the Φ_a is varying around Φ_w with a deflection

$\Delta\Phi_a$; the dc-SQUID outputs a ΔV_s like a linear flux-to-voltage convertor, as long as the $|\Delta\Phi_a|$ is smaller than a value ε ($\varepsilon < 0.5\Phi_0$), $|\Delta\Phi_a| < \varepsilon$.

The negative feedback mechanism of the FLL keeps canceling the ΔV_s , and Φ_a will be fixed at the working point dynamically, thus

$$\left. \begin{aligned} \Delta V_s + V_n &\approx 0 \\ \Delta V_s &= \frac{\partial V_s}{\partial \Phi_a} \Delta\Phi_a \\ \Delta\Phi_a &= \Phi_a - \Phi_w - n_w \Phi_0 \end{aligned} \right\} \Rightarrow \Phi_a = \Phi_w + n_w \Phi_0 - \Phi_n \quad (22)$$

where the Φ_n is the equivalent flux noised contributed by the voltage noise V_n of the room-temperature amplifier, and

$$\Phi_n = \frac{V_n}{\partial V_s / \partial \Phi_a} \quad (23)$$

Accordingly, the flux-voltage conversion function of FLL in static state is

$$\Phi_e = \Phi_f + \Phi_a = \Phi_f + \Phi_w + n_w \Phi_0 - \Phi_n \quad (24)$$

Meanwhile, to a given V_{f_FS} which is the full-scale range of V_f , the full-scale range of the input flux, namely Φ_{e_FS} will be

$$\Phi_{e_FS} = \frac{M_f}{R_f} V_{f_FS} \quad (25)$$

For a limited V_{f_FS} in the measurement instruments and a fixed M_f in the given SQUID chip, the Φ_{e_FS} is only adjusted by R_f in the practical operations.

In frequency domain, the transfer function of the FLL is defined by

$$H(\omega) = \frac{\Phi_f(\omega)}{\Phi_e(\omega)} = \frac{1}{1 + R_f / (R_{ftr} G(\omega))}; \omega > 0 \quad (26)$$

where R_{ftr} is the trans-impedance of the dc-SQUID seen from the two terminals of the feedback coil, and

$$R_{ftr} = \frac{\partial V_s}{\partial \Phi_a} M_f \quad (27)$$

This R_{ftr} is decided by the transfer coefficient of the SQUID.

From the transfer function, the cut-off frequency f_c of the FLL can be defined as

$$\left| R_f / (R_{ftr} G(\omega)) \right| = 1 \Rightarrow f_c \approx \frac{R_{ftr}}{R_f} GBP(f_c) \quad (28)$$

where $GBP(f)$ is the gain-bandwidth-product (GBP) of the room-temperature amplifier with a gain $G(\omega)$, and

$$GBP(f) = |G(\omega) f| \quad (29)$$

The maximum slew-rate, $SR_{\max}(f)$ [26], evaluates the response of the FLL to large

input of Φ_e ; the maximum swing of Φ_f driven by the room-temperature amplifier is less than $V_{spp}G(\omega)M_f/R_f$, because the maximum swing of V_s is limited by the V_{spp} . Accordingly, the maximum slew-rate of the Φ_f is limited by

$$SR_{\max}(f) \approx \pi V_{spp} \frac{M_f}{R_f} GBP(f) \quad (30)$$

The $GBP(f)$ is a constant for the room-temperature amplifier implemented by one operational amplifier or one integrator; the maximum slew rate for the FLL with a constant $GBP(f)$ is decided by the cut-off frequency f_c as [26]

$$SR_{\max}(f) \approx \frac{\pi V_{spp} f_c}{\partial V_s / \partial \Phi_a} \approx \frac{\pi \Phi_0 f_c}{2} \quad (31)$$

However, the f_c is limited by the phase-margin (PM) of the $G(\omega)$, and the PM is reduced rapidly in the cascaded amplifier; this is why we suggest to design a FLL with no more two amplifiers [24].

6.4 How to improve performances of FLL

The advantages of SQUID sensors are low noise, low drift, wide range, and high slew-rate; they are achieved by using the different readout schemes as summarized in Table 2. Those schemes can be interpreted by the transfer functions of FLL.

Table 2. Schemes to improve the performance of FLLs

Performance	Scheme	References
Low noise	1) To lower V_n of preamplifier	[46-51]
	2) To improve $\partial V_s / \partial \Phi_a$	[14],[52],[53], [54-58]
	3) Using intermediate amplifier	[25],[59-63]
Low drift	1) To reduce $1/f$ noise in Φ_n	[25], [64],[65]
	2) Suppressing the drift of Φ_w	[66-68]
Wide range	To trace the variation of n_w	[69-74]
High slew-rate	To improve $GBP(f)$	[24], [75-79]

7. Bias modes and working points

7.1 Bias and amplifier circuits

For a given dc-SQUID, the transfer coefficient depends on the location of working point in the current-voltage curves; the working point is set by room-temperature amplifier. Two schemes of the room-temperature amplifier in non-inverting and inverting modes are exhibited in Fig. 23, where dc-SQUID is read out by the preamplifier OPA1 with R_g connected between the output and the inverting input; the OPA2 is working with an open-loop gain; the GBP is modified by R_2 and C_2 .

The dc-SQUID in Fig. 23(a) is working with the preamplifier in the current-bias-voltage amplifier (VBCA) mode [80], as shown in Fig. 24(a); it shown in Fig. 23(b) is working in the voltage-bias-current-amplifier (VBCA) mode [80], as shown in Fig.

24(b). The R_{wire} is the resistance of the wire connected between the dc-SQUID and the preamplifier; the R_g is much larger than R_r , R_{wire} , as well as the shunt resistors of the dc-SQUID.

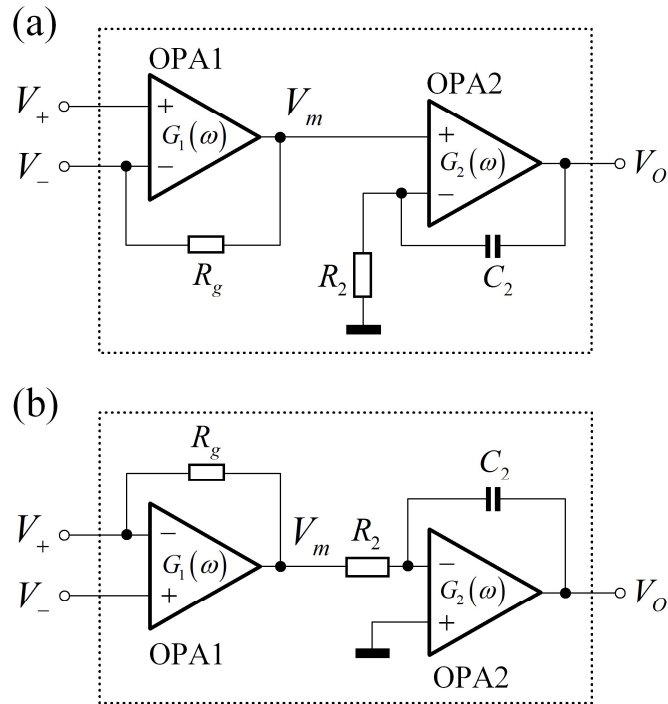


Fig. 23. Two room-temperature amplifier schemes: (a) noninverting mode, and (b) inverting mode.

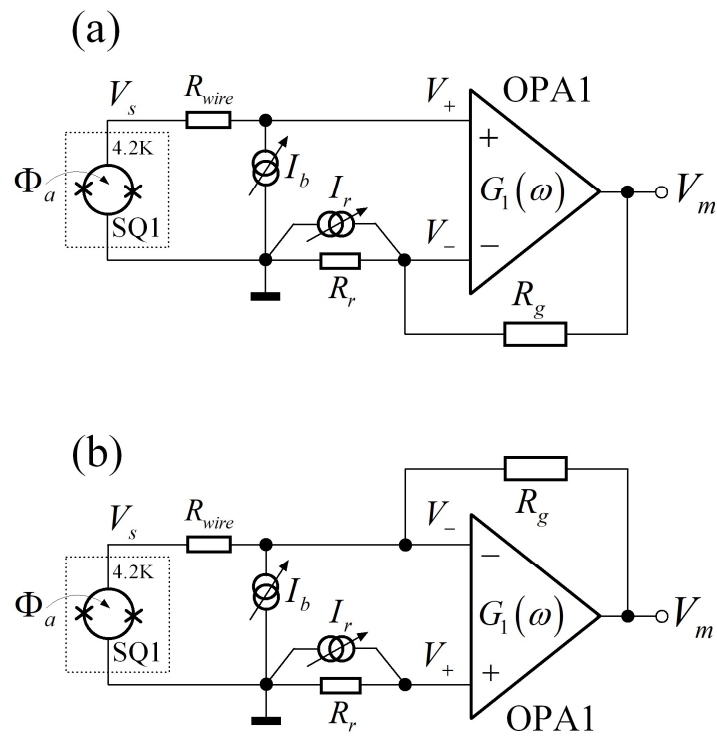


Fig. 24. Two bias-and-amplifier modes: (a) CBVA mode, and (b) VBCA mode [80].

In the CBVA mode, the V_s of the dc-SQUID under the constant bias current I_b is linearly amplified to V_m ; the transfer function from V_s to V_m is

$$\left(\frac{V_m}{R_g} + I_r\right)R_r = V_s + R_{wire}I_b \quad (32)$$

In the VBCA mode, the i_b flowing through the dc-SQUID under the bias voltage I_rR_r is linearly amplified to V_m ; the transfer function from i_b to V_m is

$$V_m/R_g + I_b = i_b \quad (33)$$

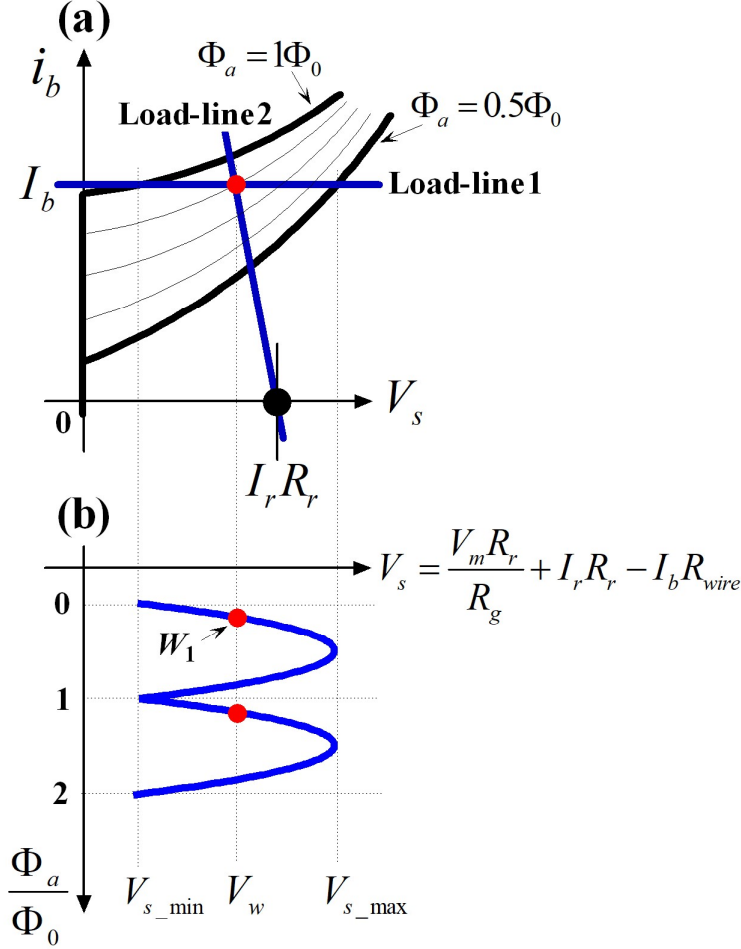


Fig. 25. Principle of CBVA mode: (a) two load lines and (b) flux-voltage characteristic [81].

7.2 Working points set by two bias modes

When the FLL based on either the CBVA or the VBCA mode is in the locking state, the output of OPA1 will be kept at zero, $V_m = 0$; the current flowing into R_g is ignored, and the i_b is totally supplied by the current source I_b ; the V_+ and V_- at two inputs of the OPA1 are equal, $V_+ = V_-$. Therefore, the working point of the dc-SQUID in either bias mode is selected by two load lines:

The first load line, which is named as Load-line1 [81], is

$$i_b = I_b \quad (34)$$

The second load lines, which is called Load-line2 [81], is

$$V_s + i_b R_{wire} = I_r R_r \quad (35)$$

Two load lines set in CBVA mode together with the current-voltage characteristics of the dc-SQUID are drawn in Fig. 25(a). The Load-line1 is moved up and down by adjusting I_b , while the Load-line2 is shifted from left to right by increasing I_r .

When the FLL is in opened-loop state, the flux-voltage characteristic of the dc-SQUID is read out by the OPA1 in CBVA mode, which is the projection of the current-voltage characteristics on the Load-line1, as illustrated in Fig. 25(b), where the intersection of two load lines is accordingly projected to the working points.

Similarly, two load lines set in VBCA mode together with the current-voltage characteristics of the dc-SQUID are drawn in Fig. 26(a). When the FLL is in opened-loop state, the OPA1 in VBCA mode reads out the flux-current characteristic of the dc-SQUID as illustrated in Fig. 26(b); it is the projection of the current-voltage characteristics on the Load-line2, and the working points is set by the intersection of two load lines.

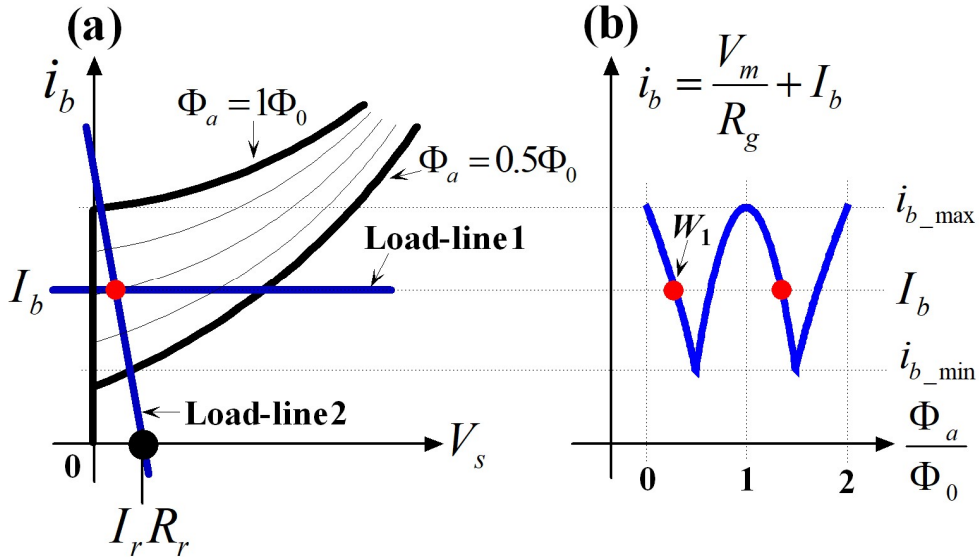


Fig. 26. Principle of VBCA mode: (a) two load lines and (b) flux-current characteristic [81].

In operations of FLL, the working point of dc-SQUID is simply set with two practical principles:

- 1) The first one is to achieve the maximum swing of V_m scanned by the input Φ_a ; the swing of V_m is adjusted by the Load-line1 in CBVA mode; it is adjusted through Load-line2 in VBCA mode.
- 2) The second one is to set the zero-baseline of V_m in the middle of the swing. The baseline of V_m is set by the Load-line2 in CBVA mode, and is adjusted by Load-line1 in VBCA mode.

By comparing Fig. 25 with Fig. 26, we can find that the working points selected by two bias modes will be in different locations in the current-voltage curves.

7.3 Small signal analyses

In either CBVA or VBCA circuit, the small-signal response of the dc-SQUID around the selected working point is described as

$$\Delta V_s = f(I_b + \Delta i_b, \Phi_w + \Delta \Phi_a) - f(I_b, \Phi_w) \approx R_d \Delta i_b + \frac{\partial V_s}{\partial \Phi_a} \Delta \Phi_a \quad (36)$$

where R_d is the dynamic resistance of the dc-SQUID working at W_1 ; it is defined by

$$R_d = \left. \frac{\partial f(i_b, \Phi_a)}{\partial i_b} \right|_{\substack{i_b = I_b \\ \Phi_a = \Phi_w + n_w \Phi_0}} \quad (37)$$

The Thevenin's equivalent circuit of the dc-SQUID in small signal mode, is equivalent to a flux-controlled voltage source in serial with an internal resistor R_d , as shown in Fig. 27. The voltage signal generated by $\Delta \Phi_a$ is amplified by a non-inverting amplifier in the CBVA scheme, as shown in Fig. 27(a), and it is amplified by an inverting amplifier in the VBCA scheme, as shown in Fig. 27(b).

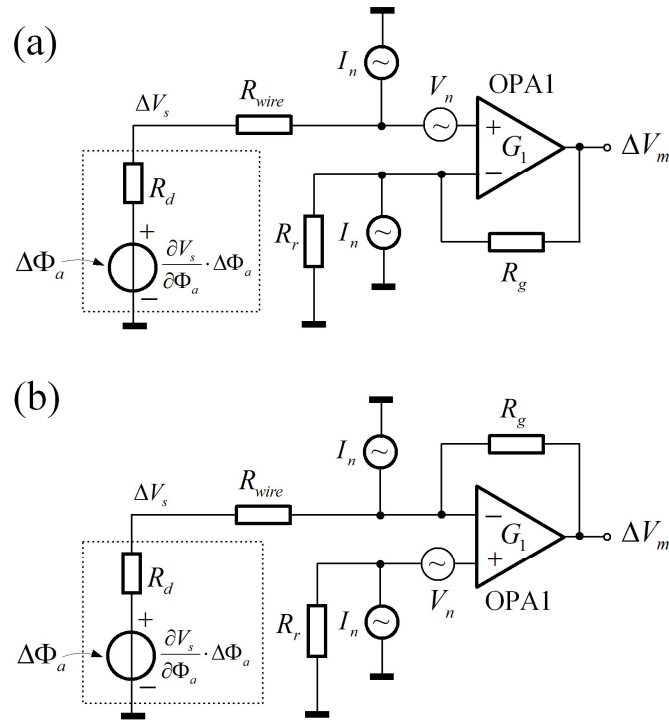


Fig. 27. Small signal circuit of dc-SQUID working (a) in CBVA mode, and (b) in VBCA mode [80].

In both CBVA and VBCA circuits, the current noise I_n and voltage noise V_n of the room-temperature preamplifier OPA1 will contribute an equivalent flux noise Φ_n to the FLL as

$$\Phi_n = \frac{\sqrt{V_n^2 + (I_n R_d + I_n R_{wire})^2 + (I_n R_r)^2}}{\partial V_s / \partial \Phi_a} \quad (38)$$

The voltage noise V_n of room-temperature amplifier is the dominant noise source, if

the R_r , R_d , and R_{wire} meet the impedance matching condition [80], namely

$$R_r < R_n; (R_d + R_{wire}) < R_n; R_n = V_n / I_n \quad (39)$$

where R_n is the so-called noise-impedance of the preamplifier.

Therefore, in both bias and amplifier modes, the Φ_n contributed by the V_n is only decided by the $\partial V_s / \partial \Phi_a$ at the selected working point.

7.4 Comparison between two bias modes: an example

In practical operations, the two bias modes will set their working points at different locations in the current-voltage curves, and will therefore achieve different noise performances, if different working points achieve different $\partial V_s / \partial \Phi_a$. For a practical dc-SQUID, we can measure its current-voltage curves as shown in Fig. 28(a); the contour map shown in Fig. 28(b) exhibits the value of $\partial V_s / \partial \Phi_a$ at each point in the current-voltage curves; the higher value of $\partial V_s / \partial \Phi_a$ is highlighted with darker color [81].

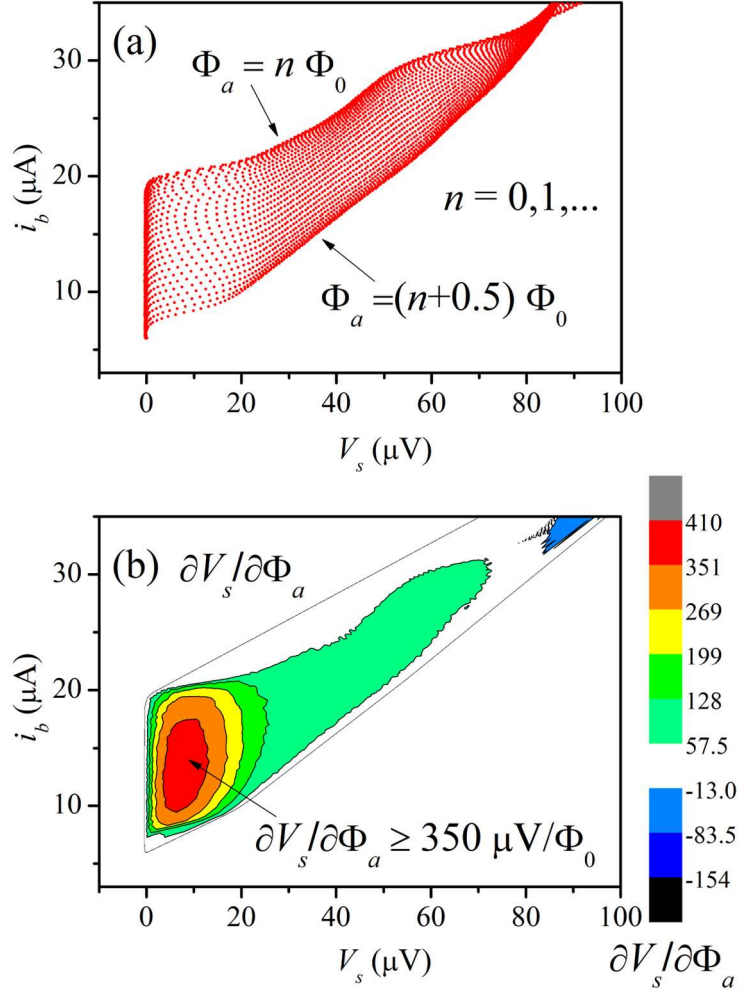


Fig. 28. (a) Current-voltage characteristics measured from a practical dc-SQUID; (b) The contour map of flux-to-voltage transfer coefficient [81].

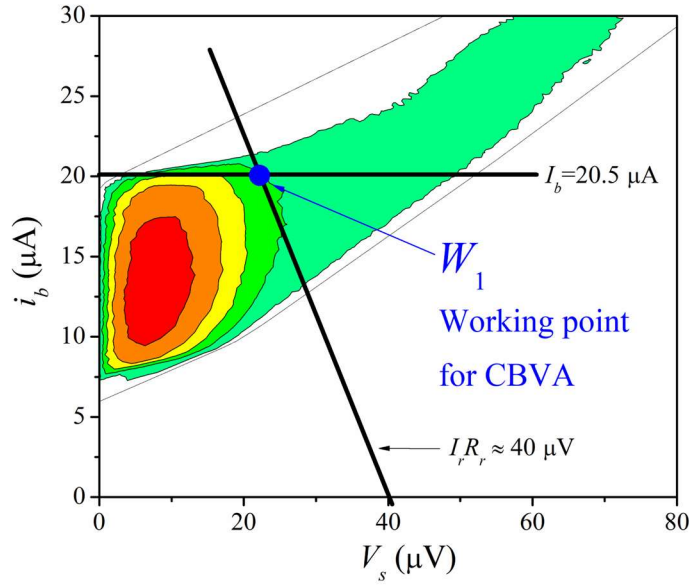


Fig. 29. Working point selected by CBVA mode [81].

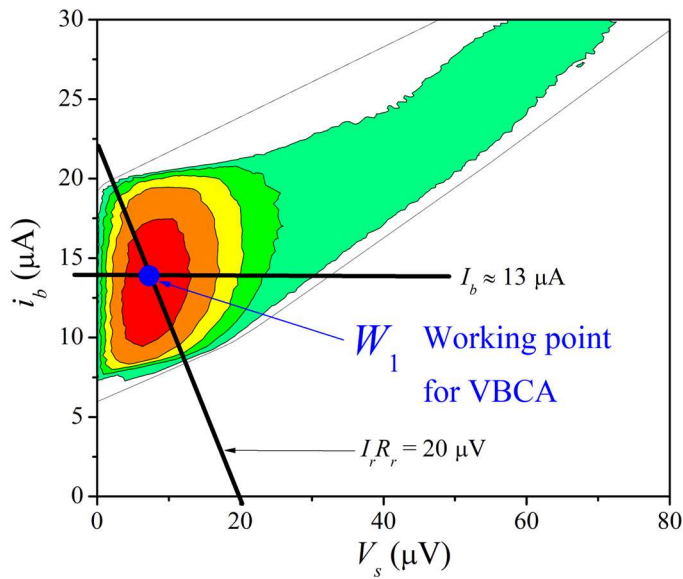


Fig. 30. Working point selected by VBCA mode [81].

Fig. 29 depicts the working point selected by the CBVA mode in the contour map, where the working point at the intersection point of two load lines is away from the area with high transfer coefficient. In the contrast, the working point selected by the VBCA mode is located in the area with high transfer coefficient, as shown Fig. 30.

The noise spectra of the FLLs in two bias schemes are compared as shown in Fig. 31. The FLL with VBCA scheme achieves better noise performance than the one with CBVA scheme, because the working point selected by the VBCA scheme achieve higher transfer coefficient than the one selected by the CBVA scheme. More details are seen in the reference [81].

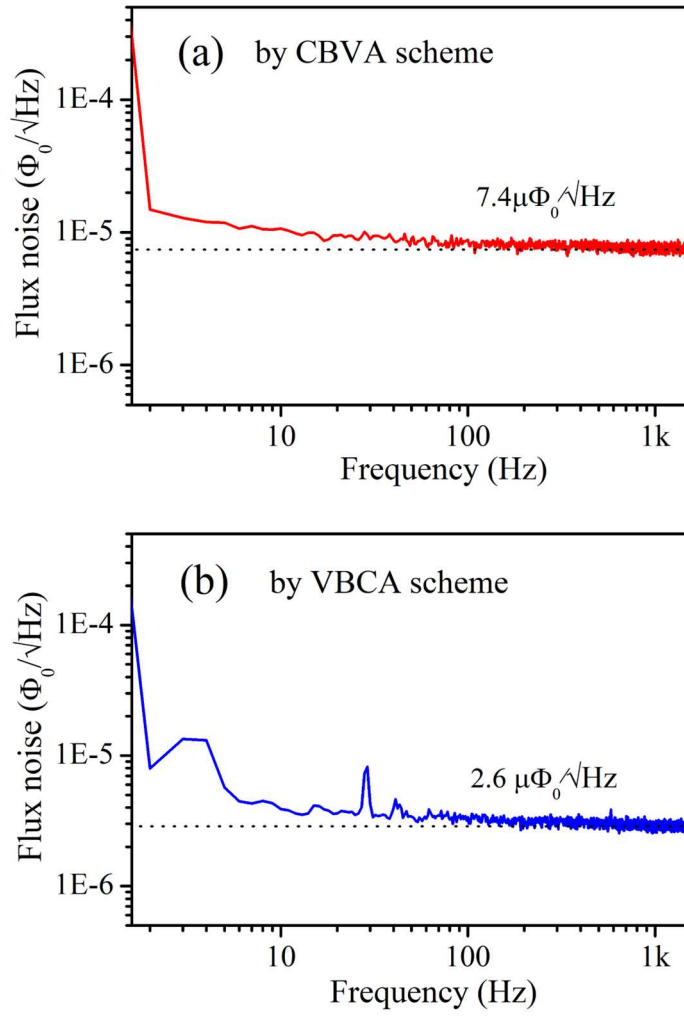


Fig. 31. (a) Noise spectrum read out by CBVA mode; (b) noise spectrum read out by VBCA mode [81].

8. Improving flux-voltage transfer coefficient

8.1 Four low-noise readout schemes

To further improve the transfer coefficient of dc-SQUID in the CBVA and VBCA circuits, the near-SQUID feedback schemes, such as additional positive feedback (APF) scheme [54], noise cancellation scheme [56], bias-current feedback (BCF) scheme [57], SQUID bootstrap circuit (SBC) scheme [58], are developed, as illustrated in Fig. 32. Four readout schemes are summarized in Table 3.

Table 3. Four direct readout schemes with near-SQUID feedback

	Near-SQUID feedback	Bias and amplifier mode
APF scheme	Voltage feedback	CBVA
NC scheme	Voltage feedback	VBCA
APF and BCF scheme	Voltage and current feedback	CBVA
SBC scheme	Voltage and current feedback	VBCA

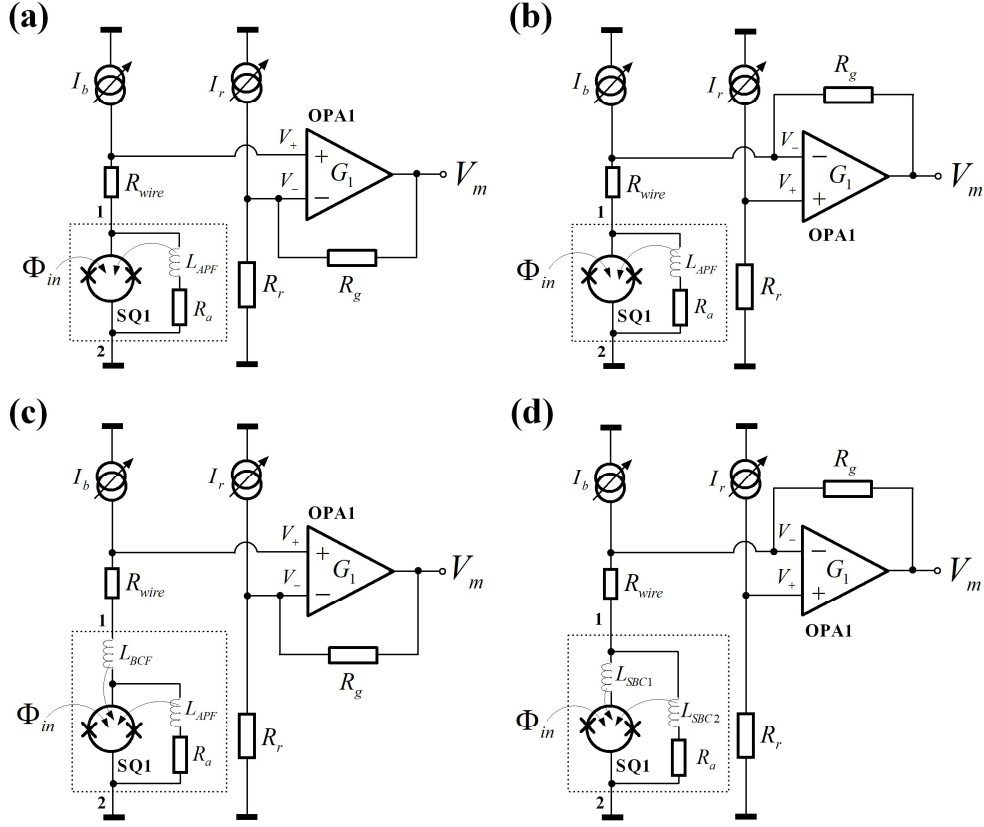


Fig. 32. Four readout schemes with near-SQUID feedback: (a) APF scheme working in CBVA mode []; (b) APF scheme working in VBCA mode []; (c) APF combined with BCF scheme working in CBVA mode []; (d) SBC scheme working in VBCA mode [80].

8.2 General equivalent circuit of near-SQUID feedback

Three kinds of near-SQUID feedback schemes in Fig. 32 are extracted and depicted in Fig. 33. Their common equivalent circuit is shown in Fig. 33(d), where the current i_b is turned into the flux $M_I i_b$ in the dc-SQUID through a mutual inductance M_I , and the voltage V_s generates the flux $M_V V_s / R_a$ to the dc-SQUID through a mutual inductance M_V . The M_I and M_V in different schemes are configured with different values as

$$\begin{bmatrix} M_I \\ M_V \end{bmatrix} = \begin{cases} \begin{bmatrix} 0 \\ M_{APF} \end{bmatrix}; & \text{in APF scheme} \\ \begin{bmatrix} M_{BCF} \\ M_{APF} \end{bmatrix}; & \text{in APF and BCF scheme} \\ \begin{bmatrix} M_{SBC1} \\ M_{SBC1} + M_{SBC2} \end{bmatrix}; & \text{in SBC scheme} \end{cases} \quad (40)$$

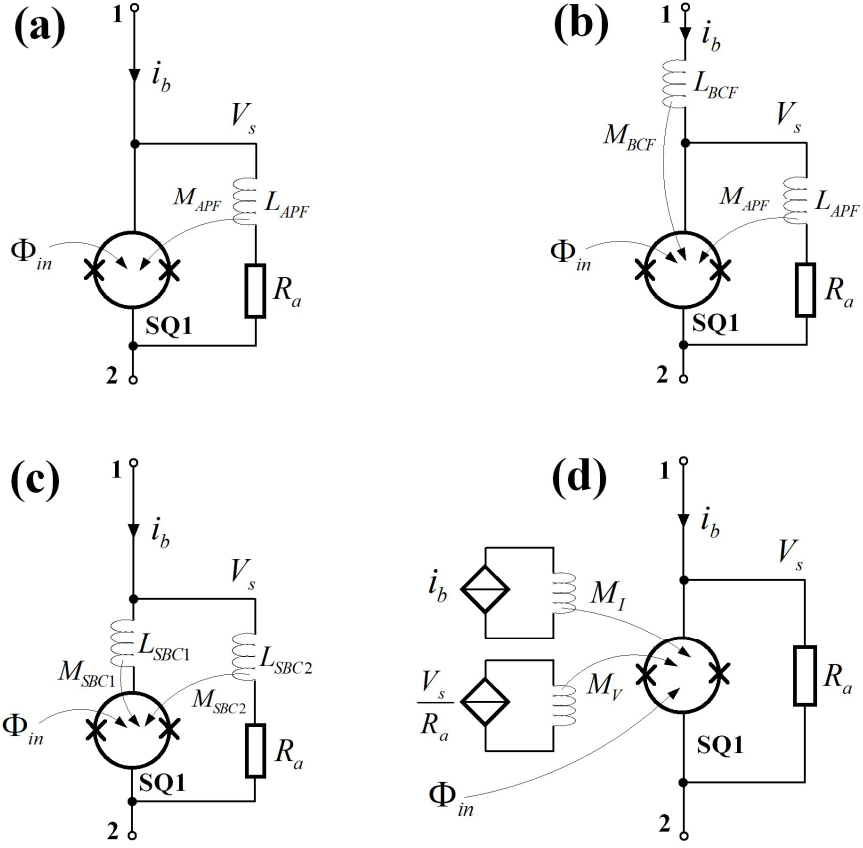


Fig. 33. Near-SQUID feedback schemes and general equivalent circuit: (a) APF scheme; (b) APF and BCF scheme; (c) SBC scheme; (d) general equivalent circuit.

8.3 Small-signal model of near-SQUID feedback circuits

In the locked FLL, the near-SQUID feedback schemes are also working in small signal mode, which small-signal circuit is shown in Fig. 34(a). The feedback effects of Δi_b and ΔV_s are equivalent to a current-controlled voltage source and a voltage-controlled voltage sources, as shown in Fig. 34(b), in which, R_I and R_V are two equivalent trans impedances [80] defined as

$$\begin{cases} R_I = \frac{\partial V_s}{\partial \Phi_a} M_I \\ R_V = \frac{\partial V_s}{\partial \Phi_a} M_V \end{cases} \quad (41)$$

The final Thevenin's equivalent circuit of the near-SQUID feedback schemes in small-signal mode is shown in Fig. 34(c). The overall transfer coefficient and the dynamic resistance are derived as follows [80]:

$$\frac{\partial V_s}{\partial \Phi_{in}} = \frac{\partial V_s}{\partial \Phi_a} \cdot \frac{1}{1 - (R_V - R_d)/R_a} \quad (42)$$

$$(R_d)^* = R_d \cdot \frac{1 - R_I/R_d}{1 - (R_V - R_d)/R_a} \quad (43)$$

where the stable condition for the feedback schemes is

$$R_I < R_d; R_V < R_d + R_a \quad (44)$$

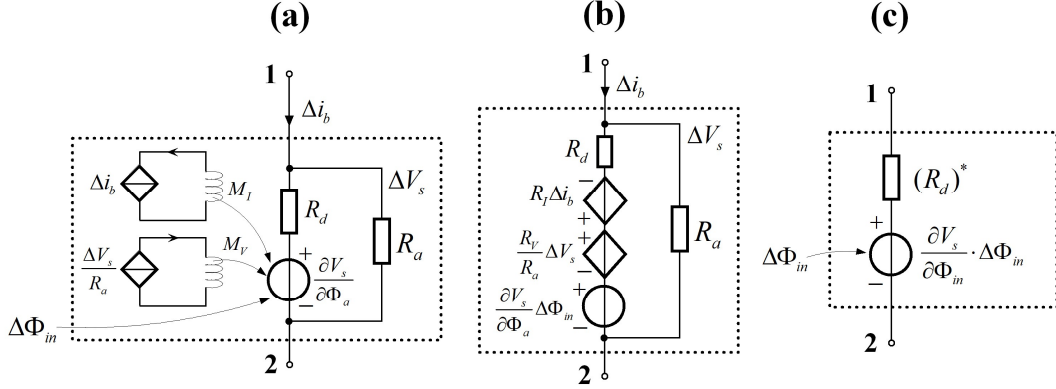


Fig. 34. (a) small-signal model of near-SQUID feedback scheme; (b) simplified equivalent circuit based on TIA model; (c) The final Thevenin's equivalent circuit [1].

We find that the near-SQUID schemes modify the transfer coefficient and dynamic resistance through two trans impedances R_I and R_V :

- 1) The R_V is the only parameter that can improve the transfer coefficient. The increase of R_V will accordingly increase both the transfer coefficient and the dynamic resistance.
- 2) The R_I has no effect on the transfer coefficient; it is only used to adjust the dynamic resistance for the noise matching condition in (39).

In summary, three near-SQUID feedback schemes are equivalent; the APF branch has the effect to increase the overall transfer coefficient, whereas the coil L_{BCF} and the coil L_{SBC1} are only useful in modifying the dynamic resistance.

9. Working point jump and flux-quanta counting

9.1 Working point shift in FLL

The working point shift in a FLL is illustrated in Fig. 35. In the flux-voltage curve of dc-SQUID, there is a threshold value Φ_{th} between Φ_w and $1\Phi_0$, where $V_s > V_w$, if $\Phi_w < \Phi_a < \Phi_{th}$, and $V_s < V_w$, if $\Phi_{th} < \Phi_a < 1\Phi_0$. If a sudden change of Φ_e move Φ_a to the region between Φ_{th} and $1\Phi_0$ (colored in yellow), as shown in Fig. 35 (a), the FLL will pull the Φ_a to W_2 , as exhibited in Fig. 35(b).

After the working point shifts from W_1 to W_2 , n_w is changed from 0 to 1, and the FLL will have a flux jump of $1\Phi_0$ in Φ_f , according to (24). A typical flux jump measured in experiments is illustrated in Fig. 36, where the jump of $1\Phi_0$ in Φ_f is resulted by one flux-quantum increasement in n_w .

Therefore, to extend the range of FLL, we can track the change of n_w , Δn_w , from the flux jumps of Φ_f , and include the Δn_w in (24) to calculate the input Φ_e . This read out method is called the flux-quantum counting (FQC) scheme [69-74].

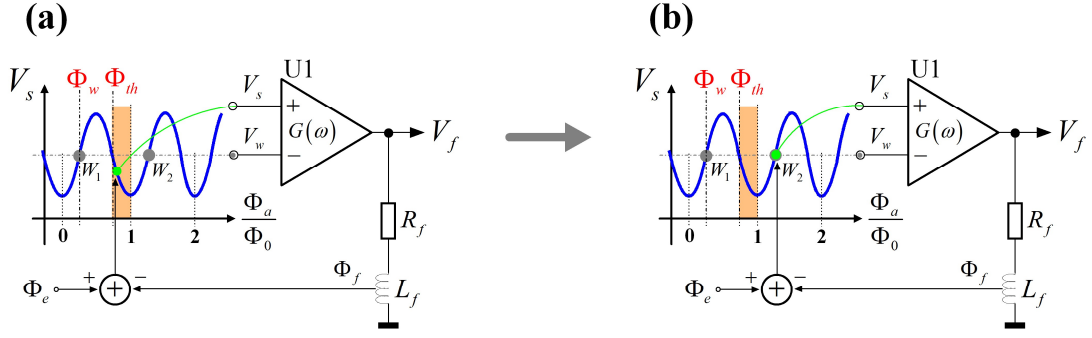


Fig. 35. Working point shift in FLL: (a) Φ_a is moved to the yellow area between Φ_{th} and Φ_0 by the sudden change of Φ_e ; (b) FLL is relocked at W_2 with a flux jump of $1\Phi_0$ in Φ_f .

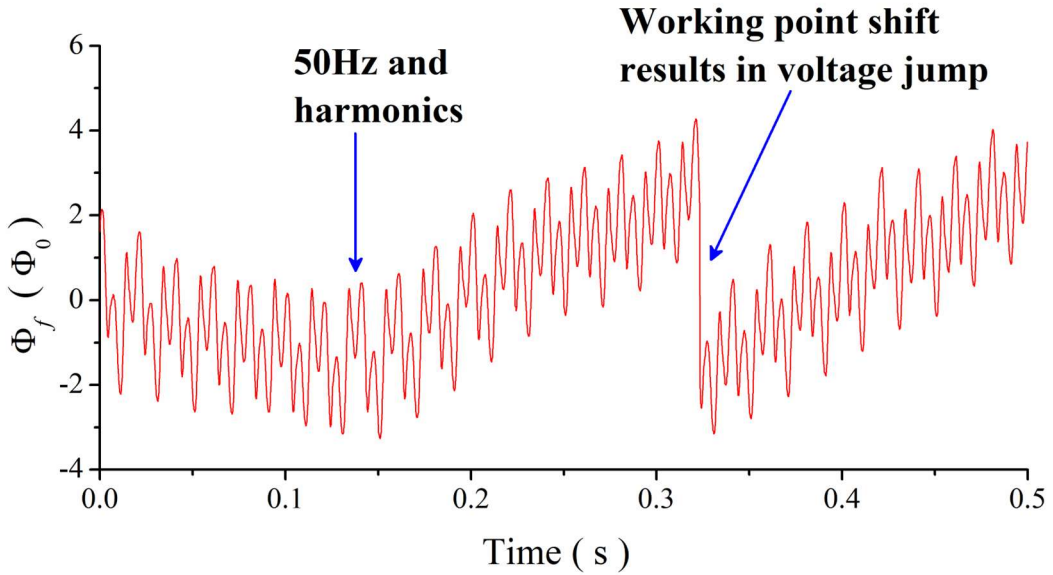


Fig. 36. A voltage-jump resulted by working point shift in a practical measurement.

9.2 Flux-quantum counting scheme

The conventional FLL reads out the Φ_e with Φ_f by assuming that the n_w in (24) remain unchanged, $\Delta n_w = 0$. If we reset the FLL intentionally when the output of FLL exceeds a threshold, and infer the Δn_w according to the flux jumps in the measured FLL output, we can extend the measurement range of Φ_e by including both the results of Δn_w and Φ_f in (24). This is exactly the principle that the conventional flux-quantum counting (FQC) readout schemes [69-71] are based to implement wide range measurements.

However, additional comparator and control circuits are used to reset the FLL; their response time is the dead time of FQC schemes, because the FQC scheme will miss counting the change of n_w during the dead time. To reduce the dead time and avoid the

miscounting of n_w , FQC schemes enhanced by simple proportional feedback are developed [73] [74]; their working point is reset automatically without any external control circuits.

9.3 Proportional feedback scheme

The proportional feedback schemes that reset the working point automatically are illustrated in Fig. 37. The one integrated with the dc-SQUID in one chip is demonstrated in Fig. 37(a), and the one implemented with a room-temperature proportional amplifier is illustrated in Fig. 37(c).

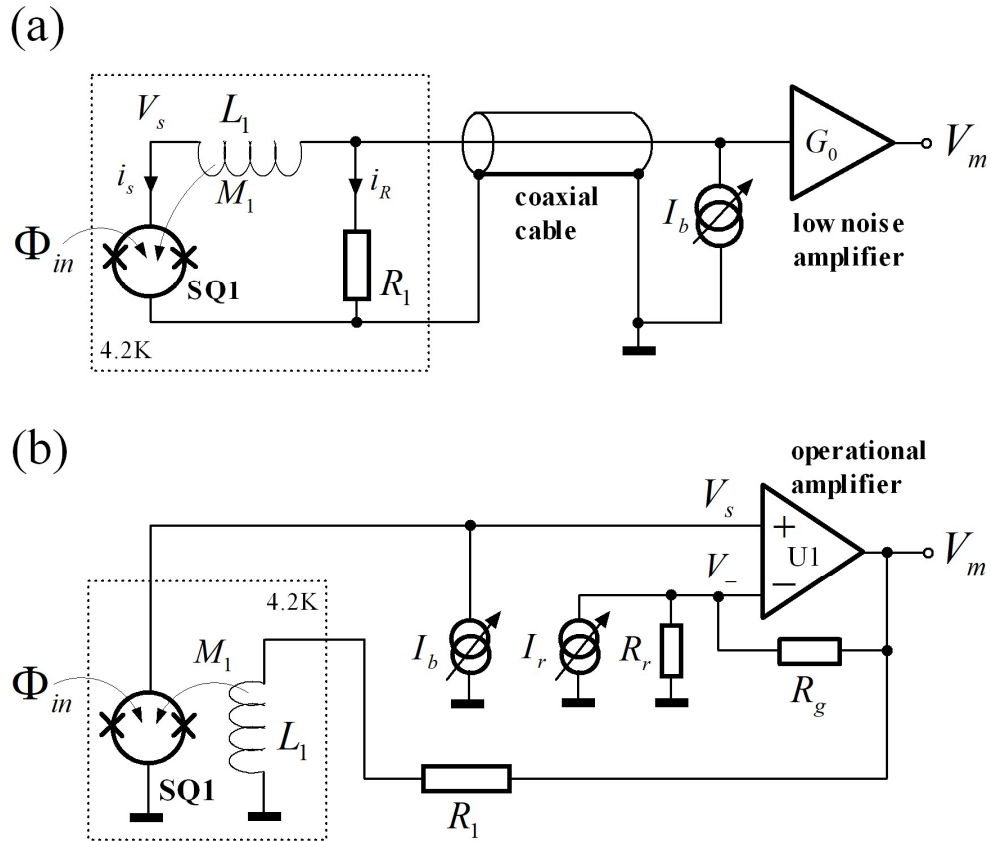


Fig. 37. Two proportional feedback schemes: (a) the one implemented with APF circuit in dc-SQUID chip [73]; (b) the one implemented with room-temperature preamplifier [74].

The proportional feedback schemes modify the flux-voltage characteristic of the dc-SQUID and narrow the Φ_{th} to $0.5\Phi_0$, as shown in Fig. 38. For a dc-SQUID with a flux-voltage curve shown in Fig. 38(a), the proportional feedback will pull the Φ_a in the region between $0.5\Phi_0$ and $1\Phi_0$ quickly back to the quasi-linear region between 0 and $0.5\Phi_0$; the region between Φ_{th} and $1\Phi_0$ is absent, and the Φ_{th} is narrowed to $0.5\Phi_0$.

If the scheme shown in Fig. 37(b) is used as the preamplifier circuit in a FLL, the proportional feedback scheme will keep the dc-SQUID working with only the quasi-linear characteristic between 0 and $0.5\Phi_0$, and will therefore reduce the response time of the FLL.

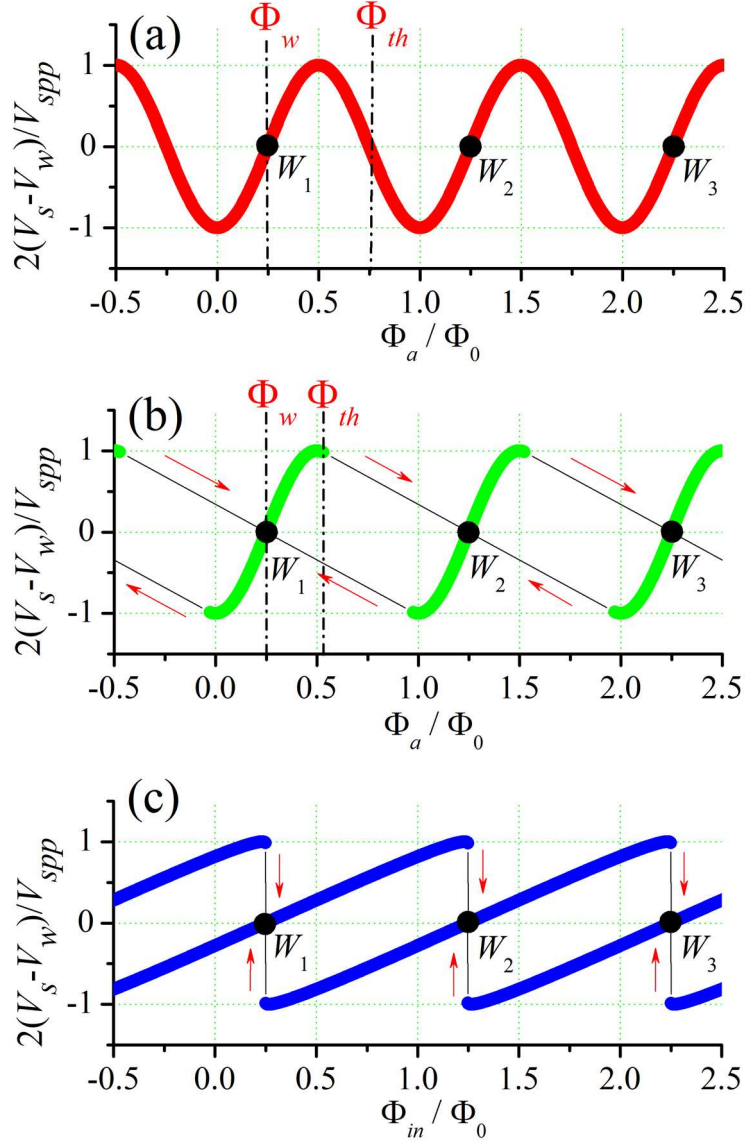


Fig. 38. (a) Original flux-voltage characteristic of dc-SQUID; (b) the flux-voltage characteristic of dc-SQUID modified by the proportional feedback scheme; (c) the overall flux-voltage characteristic read out by the proportional feedback scheme [73].

10. Other practical readout schemes

10.1 FLL with single operational amplifier

The room-temperature amplifier in the SQUID-based FF-OPA usually consists of a preamplifier and an integrator to achieve a high gain $G(\omega)$ [5], [20]. It is also implemented with a single amplifier [77] [78], as shown in Fig. 39, where the R_g used to connect the inverting input and the output of U1 is switched by SW1 [24]. When SW1 is on, the FLL is same with the readout circuit shown in Fig. 37(b), and is used to set the working point according to its flux-voltage characteristic shown in Fig. 38(c). When SW1 is off, the circuit is in closed-loop mode, and is exactly the simple flux-follower shown in Fig. 19(b).

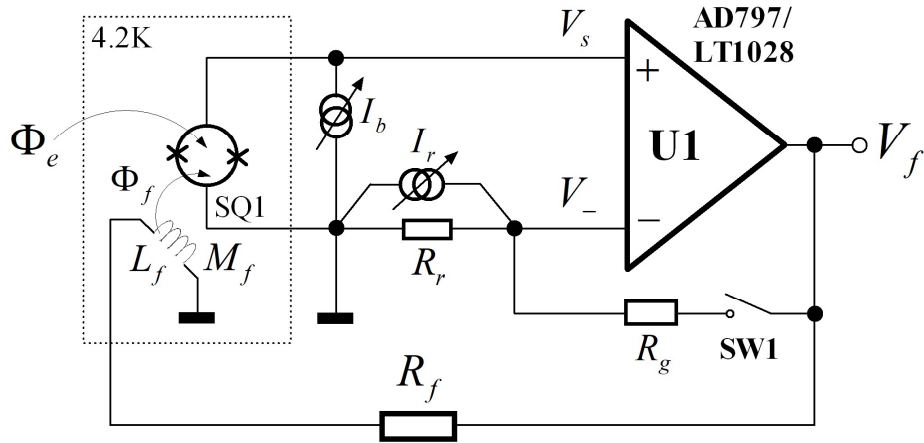


Fig. 39. Simple FLL using one operational amplifier [24].

10.2 Practical two-stage readout scheme

A practical two-stage readout scheme is exhibited in Fig. 40, where SQ1 is the first-stage dc-SQUID used to sense the flux input Φ_e , and SQ2 is the second-stage dc-SQUID used to amplify the output of SQ1 [63].

Different with the conventional two-stage schemes [59-62], our two-stage scheme improves the transfer coefficient of two-stage SQUIDs with two feedback schemes:

- 1) The first one is the APF scheme nearby SQ1; it is used to improve the transfer coefficient of SQ1.
- 2) The second one the proportional feedback scheme; it is used to enable the second-stage SQUID amplifier to achieve quasi-linear flux-voltage characteristics shown in Fig. 38(c).

Two schemes are combined to achieve an improvement of 20dB in the overall flux-to-voltage transfer coefficient, and achieve a noise floor lower than $1\mu\Phi_0/\sqrt{\text{Hz}}$. More details are seen in the reference [63].

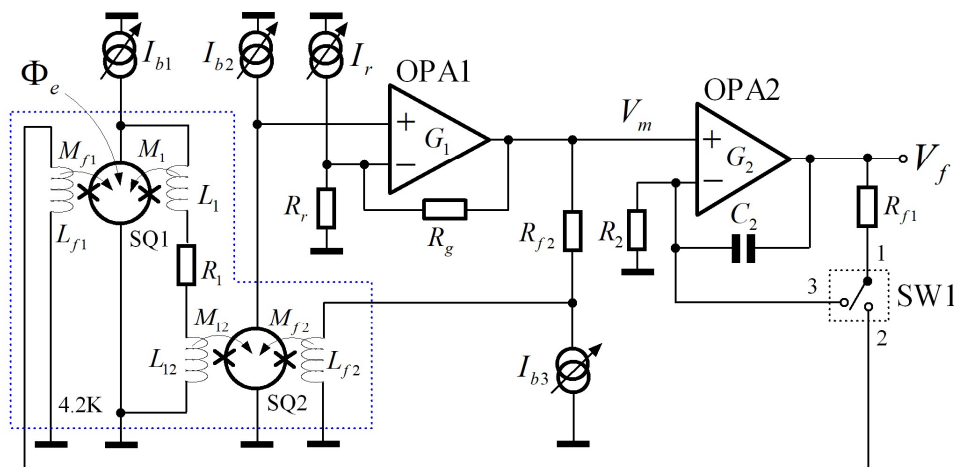


Fig. 40. FLL with two-stage SQUIDs, where SW1 is in 'off' state.

10.3 Suppression of the drift caused by the variation of R_{wire}

In the practical SQUID sensor systems that maintain cryogenic state with liquid Helium, the drop of the liquid Helium level will increase the R_{wire} in the readout circuit shown in Fig. 41(a), and make the Load-line2 shown in Fig. 25 and Fig. 26 less steep. The effects induced by the increase of R_{wire} are:

- 1) In the CBVA mode, increase of R_{wire} will move the downward zero-baseline of V_m , and arouse the dc-offset drift in Φ_f .
- 2) In the VBCA mode, increase of R_{wire} will decrease the swing of V_m , and will also induce the dc-offset drift in Φ_f .

A low differential amplifier scheme that suppresses the voltage offset created by R_{wire} is shown in Fig. 41(b). Based on this scheme, we developed a low drift and compact practical SQUID-based MCG system, as seen in reference [68].

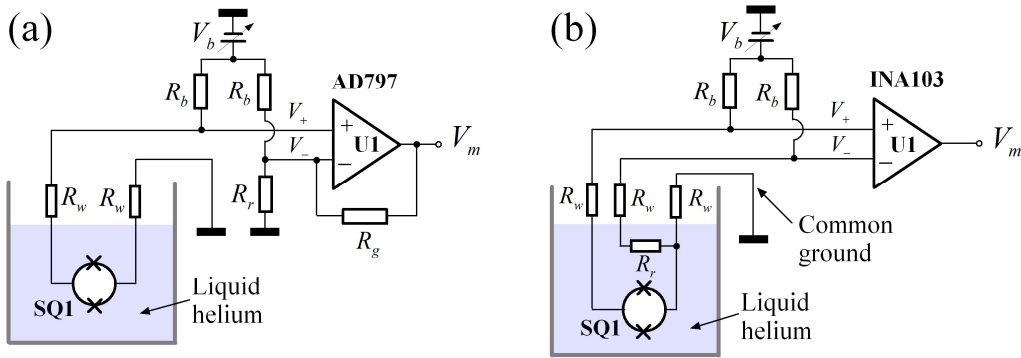


Fig. 41. Two direct readout schemes [68], where R_w is the resistance of the single wire that connects the dc-SQUID to the room-temperature amplifier: (a) scheme using single-ended amplifier; (b) scheme using differential amplifier to cancel the voltages induced by R_w .

11. SQUID-based magnetic-field sensors

11.1 Concept of trans-impedance amplifier

A linear magnetic-field sensors is simply implemented by integrating a flux-transformer to a SQUID-based flux-follower, as demonstrated in Fig. 42. In Fig. 42(a), the flux-transformer transfer the flux signal coupled by its pick-up coil to the input of the flux-follower implemented by an FF-OPA; the flux-transformer and the feedback of the flux-follower can share the same input coil, as shown in Fig. 42(b).

Viewed at two terminals of the pick-up coil, the flux-flower integrated with a pick-up coil is exactly a trans-impedance-amplifier (TIA), with which, picked-up flux signal is linearly transformed into the voltage output V_f .

the current-input MFET (CI-MFET). The scheme shown in Fig. 42(b) is implemented with the SQUID-based FF-OPA, as shown in Fig. 44, where the CI-MFET has one current input.

The CI-MFETs have current inputs as the control gate, as the MOSFETs have the voltage inputs as the control gate. The input currents modulate the current-voltage characteristics of CI-MFET, as the voltage inputs modify the current-voltage characteristics of MOSFET.

11.3 SQUID magnetic-field sensors

SQUID magnetic-field sensors are simply assembled by connecting a pick-up coil to a SQUID-based TIA, as illustrated in Fig. 45. The style of pick-up coils decides what kind of magnetic fields the SQUID magnetic-field sensor is measuring.

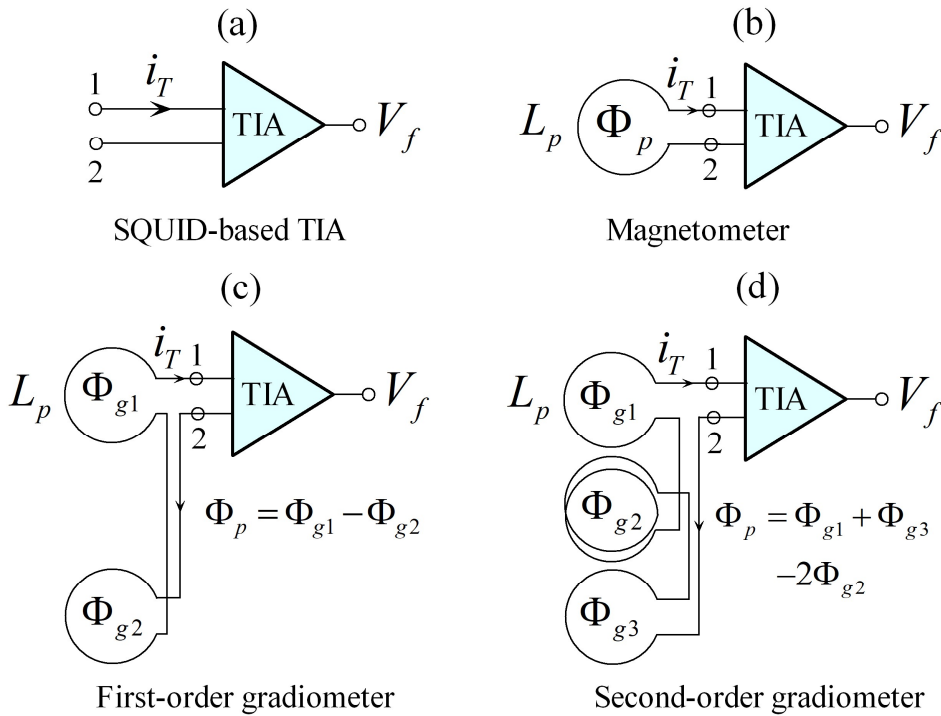


Fig. 45. SQUID sensors: (a) symbol of SQUID-based TIA; (b) magnetometer; (c) first-order gradiometer; (d) second-order gradiometer.

12. Multichannel SQUID system

12.1 Example of Multi-channel SQUID system

A Magneto-cardio-gram (MCG) system based on multi-channel SQUID sensors is exhibited in Fig 46. Excited by the heartbeats, the cardio neuro currents generate magnetic fluxes coupled by the pick-up coils. If they are modeled as a group of loop currents, j_{x1}, \dots, j_{xQ} , the MCG system is exactly a contactless multi-channel current measurement system, which senses the target currents through mutual inductances, and turns them linearly into voltage outputs.

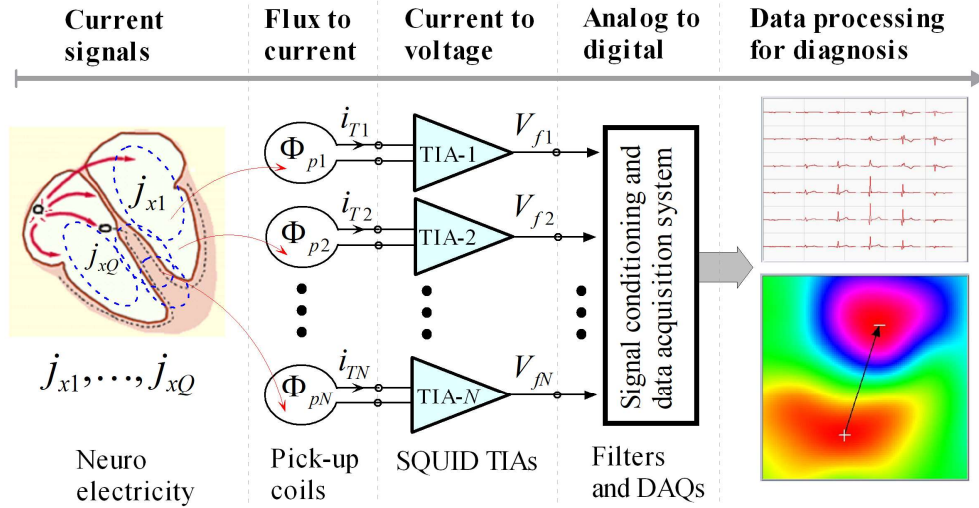


Fig. 46. A multichannel SQUID system for magnetocardiogram.

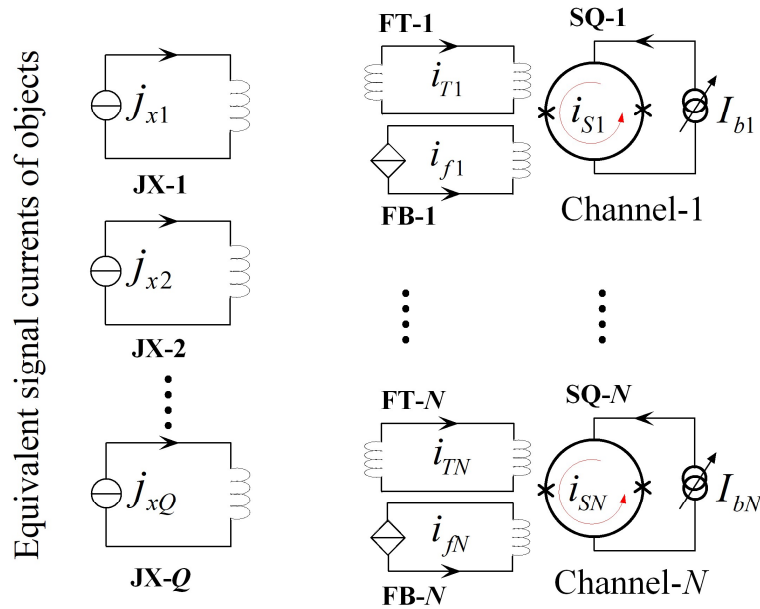


Fig. 47. General equivalent circuit of multi-channel SQUID sensors.

12.2 Equivalent circuit of multichannel SQUID system

The equivalent circuit of the multichannel SQUID system is shown in Fig. 47. It is composed of five groups of mutually-coupled current loops.

- 1) The first group of current loops, JX-1, ..., JX-Q, are assumed to generate the target magnetic fields coupled by the pick-up coils. They contain the currents circulating inside the object under test, namely j_{x1}, \dots, j_{xQ} .
- 2) The second group of current loops, FT-1, ..., FT-N, are the flux transformers, their superconducting loop currents, i_{T1}, \dots, i_{TN} , are linearly induced by the fluxes coupled by the loops.

- 3) The third group of current loops, FB-1, ..., FB- N , are the flux-feedback loops driven by the feedback currents, i_{f1} , ..., i_{fN} .
- 4) The fourth group of current loops, SQ-1, ..., SQ- N , are the dc-SQUID loops which inside contain superconducting currents, i_{s1} , ..., i_{sN} .
- 5) The fifth group of current loops are the current-biasing loops driven by the external current sources, I_{b1} , ..., I_{bN} .

<p>(a)</p> $\mathbf{M}_{\text{XS}} = \begin{matrix} & j_{x1} & \cdots & j_{xQ} \\ \text{SQ-1} & \left[\begin{matrix} M_{xS11} & \cdots & M_{xS1Q} \\ \vdots & \ddots & \vdots \\ \text{SQ-N} & \left[\begin{matrix} M_{xSN1} & \cdots & M_{xSNQ} \end{matrix} \right] \end{matrix} \right.$ <p>M_{xSij} : mutual-inductance on SQ-i by j_{xj}</p>	<p>(b)</p> $\mathbf{M}_{\text{FS}} = \begin{matrix} & i_{f1} & \cdots & i_{fN} \\ \text{SQ-1} & \left[\begin{matrix} M_{fS11} & \cdots & M_{fS1N} \\ \vdots & \ddots & \vdots \\ \text{SQ-N} & \left[\begin{matrix} M_{fSN1} & \cdots & M_{fSNN} \end{matrix} \right] \end{matrix} \right.$ <p>M_{fSij} : mutual-inductance on SQ-i by i_{fj}</p>
<p>(c)</p> $\mathbf{M}_{\text{bS}} = \begin{matrix} & I_{b1} & \cdots & I_{bN} \\ \text{SQ-1} & \left[\begin{matrix} M_{bS11} & \cdots & M_{bS1N} \\ \vdots & \ddots & \vdots \\ \text{SQ-N} & \left[\begin{matrix} M_{bSN1} & \cdots & M_{bSNN} \end{matrix} \right] \end{matrix} \right.$ <p>M_{bSij} : mutual-inductance on SQ-i by I_{bj}</p>	<p>(d)</p> $\mathbf{M}_{\text{TS}} = \begin{matrix} & i_{T1} & \cdots & i_{TN} \\ \text{SQ-1} & \left[\begin{matrix} M_{TS11} & \cdots & M_{TS1N} \\ \vdots & \ddots & \vdots \\ \text{SQ-N} & \left[\begin{matrix} M_{TSN1} & \cdots & M_{TSNN} \end{matrix} \right] \end{matrix} \right.$ <p>M_{TSij} : mutual-inductance on SQ-i by i_{Tj}</p>

Fig. 48. Mutual inductances applied to SQUIDS. (a) Mutual inductances from signal sources; (b) mutual inductances from feedback coils; (c) mutual inductances from bias currents; (d) mutual inductances from flux transformers.

<p>(a)</p> $\mathbf{M}_{\text{XT}} = \begin{matrix} & j_{x1} & \cdots & j_{xQ} \\ \text{FT-1} & \left[\begin{matrix} M_{xT11} & \cdots & M_{xT1Q} \\ \vdots & \ddots & \vdots \\ \text{FT-N} & \left[\begin{matrix} M_{xTN1} & \cdots & M_{xTNQ} \end{matrix} \right] \end{matrix} \right.$ <p>M_{xTij} : mutual-inductance on FT-i by j_{xj}</p>	<p>(b)</p> $\mathbf{M}_{\text{FT}} = \begin{matrix} & i_{f1} & \cdots & i_{fN} \\ \text{FT-1} & \left[\begin{matrix} M_{fT11} & \cdots & M_{fT1N} \\ \vdots & \ddots & \vdots \\ \text{FT-N} & \left[\begin{matrix} M_{fTN1} & \cdots & M_{fTNN} \end{matrix} \right] \end{matrix} \right.$ <p>M_{fTij} : mutual-inductance on FT-i by i_{fj}</p>
<p>(c)</p> $\mathbf{M}_{\text{bT}} = \begin{matrix} & I_{b1} & \cdots & I_{bN} \\ \text{FT-1} & \left[\begin{matrix} M_{bT11} & \cdots & M_{bT1N} \\ \vdots & \ddots & \vdots \\ \text{FT-N} & \left[\begin{matrix} M_{bTN1} & \cdots & M_{bTNN} \end{matrix} \right] \end{matrix} \right.$ <p>M_{bTij} : mutual-inductance on FT-i by I_{bj}</p>	<p>(d)</p> $\mathbf{M}_{\text{ST}} = \begin{matrix} & i_{S1} & \cdots & i_{SN} \\ \text{FT-1} & \left[\begin{matrix} M_{TS11} & \cdots & M_{TS1N} \\ \vdots & \ddots & \vdots \\ \text{FT-N} & \left[\begin{matrix} M_{TSN1} & \cdots & M_{TSNN} \end{matrix} \right] \end{matrix} \right. = \mathbf{M}_{\text{TS}}$ <p>M_{TSij} : mutual-inductance on FT-i by i_{Sj}</p>
<p>(e)</p> $\mathbf{L}_{\text{T}} = \begin{matrix} & i_{T1} & \cdots & i_{TN} \\ \text{FT-1} & \left[\begin{matrix} L_{T11} & \cdots & L_{T1N} \\ \vdots & \ddots & \vdots \\ \text{FT-N} & \left[\begin{matrix} L_{TN1} & \cdots & L_{TNN} \end{matrix} \right] \end{matrix} \right. ; L_{Tij} = \begin{cases} L_{pi} + L_{ij}, i = j : \text{self-inductance of FT-}i \\ -M_{Tij}, i \neq j : \text{mutual-inductance between FT-}i \text{ and FT-}j \end{cases}$	

Fig. 49. Mutual inductances applied to flux transformers. (a) Mutual inductances from signal sources; (b) mutual inductances from feedback coils; (c) mutual inductances from bias currents; (d) mutual inductances from SQUID loops; (e) mutual inductances between flux transformers.

Those loops are coupled through mutual inductances. Four mutual inductance matrices for the SQUID loops are defined in Fig. 48. Five mutual inductances for the flux transformers are defined in Fig. 49.

12.3 Transfer function of multichannel SQUID system

Three current vectors for the target currents, feedback currents, and bias currents, are defined in Fig. 50(a); the vectors of superconducting currents and trapped fluxes in flux transformers are defined in Fig. 50(b). The circulating currents and the applied fluxes inside SQUID loops are defined in Fig. 50(c), where the i_s in a given dc-SQUID is decided by the I_b and Φ_a . The Φ_a achieves a fixed value as defined in (22) when the FLL is locked, and an unknown value when the FLL is unlocked.

(a) Vector of current sources (b) Vector of flux transformers

$$\begin{aligned} \mathbf{j}_x &= [j_{x1} \quad \cdots \quad j_{xQ}]^T & \mathbf{i}_T &= [i_{T1} \quad \cdots \quad i_{TN}]^T \\ \mathbf{i}_f &= [i_{f1} \quad \cdots \quad i_{fN}]^T & \mathbf{n}_T &= [n_{T1} \quad \cdots \quad n_{TN}]^T \\ \mathbf{I}_b &= [I_{b1} \quad \cdots \quad i_{bN}]^T \end{aligned}$$

(c) Vector of SQUID loops

$$\begin{aligned} \mathbf{i}_s &= [i_{s1} \quad \cdots \quad i_{sN}]^T; i_{si} = \frac{1}{T} \int_0^T i_{circi} \cdot dt = f_{circi}(I_{bi}, \Phi_{ai}); i \in [1, N] \\ \Phi_a &= [\Phi_{a1} \quad \cdots \quad \Phi_{aN}]^T; \Phi_{ai} = \begin{cases} \Phi_{wi} + n_{wi} \Phi_0 - \Phi_{mi} & : \text{FLL is locked} \\ \text{unknown} & : \text{FLL is opened} \end{cases} \end{aligned}$$

Fig. 50. (a) Current vectors of current sources. (b) current and flux vectors of flux transformers. (c) current and flux vectors of SQUIDs.

According to the FQL, the flux-current relations for flux transformers are written in matrix as

$$\mathbf{M}_{xT} \mathbf{j}_x + \mathbf{M}_{fT} \mathbf{i}_f + \mathbf{L}_T \mathbf{i}_T - \mathbf{M}_{bT} \mathbf{I}_b - \mathbf{M}_{TS} \mathbf{i}_s = \mathbf{n}_T \Phi_0 \quad (45)$$

Meanwhile, the total fluxes applied to SQUID loops is expressed in matrix as

$$\mathbf{M}_{xs} \mathbf{j}_x + \mathbf{M}_{fs} \mathbf{i}_f - \mathbf{M}_{TS} \mathbf{i}_T - \mathbf{M}_{bs} \mathbf{I}_b = \Phi_a \quad (46)$$

Therefore, the transfer function of the mutual-channel SQUID system is derived as

$$\begin{aligned} \mathbf{i}_f &= (\mathbf{M}_{fs} + \mathbf{M}_{TS} \mathbf{L}_T^{-1} \mathbf{M}_{fT})^{-1} (\Phi_a + \mathbf{M}_{TS} \mathbf{L}_T^{-1} \mathbf{n}_T \Phi_0) \\ &+ (\mathbf{M}_{fs} + \mathbf{M}_{TS} \mathbf{L}_T^{-1} \mathbf{M}_{fT})^{-1} \mathbf{M}_{TS} \mathbf{L}_T^{-1} \mathbf{M}_{TS} \mathbf{i}_s \\ &+ (\mathbf{M}_{fs} + \mathbf{M}_{TS} \mathbf{L}_T^{-1} \mathbf{M}_{fT})^{-1} (\mathbf{M}_{bs} + \mathbf{M}_{TS} \mathbf{L}_T^{-1} \mathbf{M}_{bT}) \mathbf{I}_b \\ &- (\mathbf{M}_{fs} + \mathbf{M}_{TS} \mathbf{L}_T^{-1} \mathbf{M}_{fT})^{-1} (\mathbf{M}_{xs} + \mathbf{M}_{TS} \mathbf{L}_T^{-1} \mathbf{M}_{xT}) \mathbf{j}_x \end{aligned} \quad (47)$$

For SQUID sensors without flux transformers, the transfer function is simplified as

$$\mathbf{i}_f = \mathbf{M}_{fs}^{-1} (\Phi_a + \mathbf{M}_{bs} \mathbf{I}_b - \mathbf{M}_{xs} \mathbf{j}_x) \quad (48)$$

Therefore, the feedback currents are the linear projection of the target currents together with other loop currents. The crosstalk factors between SQUID sensors are induced by multiple mutual-inductance matrices. Since the calibration of those crosstalk factors through experiments is a heavy task [82], [83], the transfer functions in (47) and (48) can be used to calculate crosstalk factors with mutual inductances extracted according to the practical geometric dimensions of SQUID sensors.

13. Conclusion

We presented a comprehensive introduction to SQUID sensors, ranged from basic principles of superconductor elements to the general transfer function of multi-channel SQUID systems. SQUID sensors are the analog ‘integrated’ circuits of superconducting devices and semiconductor amplifiers working in different working temperatures. The understandings of SQUIDs and SQUID sensors are:

- 1) Superconductor and normal RLC circuits share the same circuit laws and analysis methods, except that the macroscopic phase or the integral of voltage will be used to define Josephson currents.
- 2) Flux-transformers are superconducting inductance loops wired by pure superconductor wires; SQUIDs are the superconducting RLC networks driven by Josephson currents. A flux-transformer is a linear flux-to-current convertor; a dc-SQUID is a MFET with flux-modulated current-voltage characteristics.
- 3) SQUID sensors are the linear flux- and current-based analog circuits, while MOSFET amplifiers are the linear charge- and voltage-based analog circuits.
- 4) A flux-follower implemented by the SQUID-based FF-OPAs is exactly the SQUID-based FLL.
- 5) A dc-SQUID can be read out by either CBVA or VBCA modes in a FLL. The VBCA mode will be better than the CBVA mode in selecting a working point.
- 6) Three near-SQUID feedback schemes are equivalent for improving the transfer coefficient of dc-SQUID.
- 7) A SQUID-based TIA is a flux-follower tightly coupled by an input coil. A SQUID sensor is a SQUID-based TIA connected to a pick-up coil.
- 8) A multi-channel SQUID sensor system, is a contactless current measurement system, where SQUID sensors read out the circuits circulating inside the target under test, through mutual inductances.

In summary, a dc-SQUID is a two-port RLC network driven by two Josephson currents; it is used as a MFET with flux-modulated current-voltage characteristics in FF-OPAs; a SQUID-based TIA is an FF-OPA coupled with an input coil; a SQUID sensor is a SQUID-based TIA connected with a pick-up coil. Multi-channel SQUID sensors are contactless current amplifiers. SQUID-based MFETs are dual to semiconductor FETs, in the design of analog circuits and systems.

References

- [1] W. Meissner and R. Ochsenfeld, "Short initial announcements.," (in German), *Naturwissenschaften*, vol. 21, no. 1, pp. 787-788, 1933.
- [2] B. D. Josephson, "Possible New Effects in Superconductive Tunnelling," *Physics Letters*, vol. 1, no. 7, pp. 251-253, 1962.
- [3] P. Seidel, *Applied Superconductivity: Handbook on Devices and Applications*. Weinheim, Germany: Wiley-VCH Verlag GmbH & Co.KGaA, 2015, pp. 949-1200.
- [4] H. Weinstock, *SQUID sensors: fundamentals, fabrication and applications*. Springer Science & Business Media, 2012.
- [5] J. Clarke and A. I. Braginski, *The SQUID Handbook: Fundamentals and Technology of SQUIDs and SQUID Systems Vol. I*. New York: Wiley, 2004, pp. 1-127.
- [6] K. K. Likharev and V. K. Semenov, "RSFQ logic/memory family: a new Josephson-junction technology for sub-terahertz-clock-frequency digital systems," *IEEE Transactions on Applied Superconductivity*, vol. 1, no. 1, pp. 3-28, 1991.
- [7] D. S. Holmes, A. L. Ripple, and M. A. Manheimer, "Energy-Efficient Superconducting Computing—Power Budgets and Requirements," *IEEE Transactions on Applied Superconductivity*, vol. 23, no. 3, pp. 1701610-1701610, 2013.
- [8] J. M. Martinis, M. H. Devoret, and J. Clarke, "Quantum Josephson junction circuits and the dawn of artificial atoms," *Nature Physics*, vol. 16, no. 3, pp. 234-237, 2020.
- [9] U. Vool and M. Devoret, "Introduction to quantum electromagnetic circuits," *International Journal of Circuit Theory and Applications*, vol. 45, no. 7, pp. 897-934, Jul 2017.
- [10] A. H. Silver and J. E. Zimmerman, "Quantum States and Transitions in Weakly Connected Superconducting Rings," *Physical Review*, vol. 157, no. 2, pp. 317-341, 1967.
- [11] R. C. Jaklevic, J. Lambe, A. H. Silver, and J. E. Mercereau, "Quantum Interference Effects in Josephson Tunneling," *Physical Review Letters*, vol. 12, no. 7, pp. 159-160, 1964.
- [12] J. E. Zimmerman and A. H. Silver, "Macroscopic Quantum Interference Effects through Superconducting Point Contacts," *Physical Review*, vol. 141, no. 1, pp. 367-375, 1966.
- [13] V. K. Kornev, I. I. Soloviev, N. V. Klenov, and O. A. Mukhanov, "Bi-SQUID: a novel linearization method for dc SQUID voltage response," *Superconductor Science and Technology*, vol. 22, no. 11, 2009.
- [14] D. J. Adelerhof, H. Nijstad, J. Flokstra, and H. Rogalla, "Relaxation oscillation SQUIDs with high $\delta V / \delta \Phi$," (in English), *IEEE Transactions on Applied Superconductivity*, vol. 3, no. 1, pp. 1862-1865, Mar 1993.
- [15] P. Caputo, J. Oppenlander, C. Haussler *et al.*, "High-performance magnetic field sensor based on superconducting quantum interference filters," *Applied Physics Letters*, vol. 85, no. 8, pp. 1389-1391, Aug 23 2004.
- [16] R. P. Welty and J. M. Martinis, "A series array of DC SQUIDs," *IEEE Transactions on Magnetics*, vol. 27, no. 2, pp. 2924-2926, 1991.
- [17] K. Sternickel and A. I. Braginski, "Biomagnetism using SQUIDs: status and perspectives," *Superconductor Science and Technology*, vol. 19, no. 3, pp. S160-S171, 2006.
- [18] J. Clarke, Y.-H. Lee, and J. Schneiderman, "Focus on SQUIDs in Biomagnetism," *Superconductor Science and Technology*, vol. 31, no. 8, 2018.

- [19] R. Stolz, M. Schmelz, V. Zakosarenko *et al.*, "Superconducting sensors and methods in geophysical applications," *Superconductor Science & Technology*, vol. 34, no. 3, Mar 2021.
- [20] D. Drung, "High-Tc and low-Tc dc SQUID electronics," *Superconductor Science and Technology*, vol. 16, no. 12, pp. 1320-1336, 2003.
- [21] T. Michael, *Introduction to Superconductivity: Second Edition*. New York: McGraw-Hill, Inc, 1996, pp. 110-130.
- [22] D. E. McCumber, "Effect of ac Impedance on dc Voltage-Current Characteristics of Superconductor Weak-Link Junctions," *Journal of Applied Physics*, vol. 39, no. 7, pp. 3113-3118, 1968.
- [23] Y. L. Wang, "Frequency-phase-locking mechanism inside DC SQUIDs and the analytical expression of current-voltage characteristics," (in English), *Physica C-Superconductivity and Its Applications*, vol. 609, Jun 15 2023.
- [24] Y. L. Wang, G. F. Zhang, X. F. Xu *et al.*, "Flux Feedback Amplifier based on Superconducting Quantum Interference Device," (in English), *Physica C-Superconductivity and Its Applications*, vol. 565, Oct 15 2019.
- [25] R. L. Forgacs and A. Warnick, "Digital-Analog Magnetometer Utilizing Superconducting Sensor," *Review of Scientific Instruments*, vol. 38, no. 2, pp. 214-220, 1967.
- [26] Y. L. Wang, "Study on the Circuit Technologies of SQUID Sensor for Practical Applications," Doctor of Engineering, Department of Automation, University of Science and Technology of China, Hefei 230027, China, 2021.
- [27] B. Razavi, *Design of Analog CMOS Integrated Circuits*. New York, United States of America: McGraw-Hill Education, 2017, pp. 1-44.
- [28] C. K. Alexander, M. N. Sadiku, and M. Sadiku, *Fundamentals of electric circuits*. McGraw-Hill New York, 2009, pp. 1-174.
- [29] Y. L. Wang, "An Electromagnetic-Flux-Distribution Model for Analyses of Superconducting Josephson Junction Circuits and Quantum Phase-Slip Junction Circuits," *IEEE Transactions on Applied Superconductivity*, vol. 32, no. 5, pp. 1-6, Aug 2022.
- [30] H. H. Zappe and B. S. Landman, "Analysis of resonance phenomena in Josephson interferometer devices," *Journal of Applied Physics*, vol. 49, no. 1, pp. 344-350, 1978.
- [31] D. B. Tuckerman and J. H. Magerlein, "Resonances in symmetric Josephson interferometers," *Applied Physics Letters*, vol. 37, no. 2, pp. 241-243, 1980.
- [32] S. M. Faris and E. A. Valsamakis, "Resonances in superconducting quantum interference devices—SQUID's," *Journal of Applied Physics*, vol. 52, no. 2, pp. 915-920, 1981.
- [33] Y. Wang, G. Zhang, S. Zhang, and X. Xie, "Analysis of LC-Resonance in DC SQUID Using Dynamic System Model," *IEEE Transactions on Applied Superconductivity*, vol. 30, no. 8, pp. 1-7, 2020.
- [34] Y. L. Wang, "Unified Network Equation for Both Normal RLC Circuits and Josephson Junction Circuits," *arXiv:2109.12476*, pp. 1-7, 2021.
- [35] Y. L. Wang, "Magnetic-Flux-Flow Diagrams for Design and Analysis of Josephson Junction Circuits," *IEEE Transactions on Applied Superconductivity*, vol. 33, no. 7, pp. 1-8, 2023.
- [36] Y. L. Wang, "A general flux-Based Circuit Theory for Superconducting Josephson Junction Circuits," *arXiv:2308.01693*, pp. 1-35, 2023.
- [37] R. L. Peterson and D. G. McDonald, "Voltage and current expressions for a two-junction superconducting interferometer," *Journal of Applied Physics*, vol. 54, no. 2, pp. 992-996, 1983.

- [38] J. Schambach, H. G. Meyer, L. Warzemann *et al.*, "Analytical calculation of the I-V characteristics of SQUIDs with parasitic elements," *Superconductor Science & Technology*, vol. 9, no. 8, pp. 617-621, Aug 1996.
- [39] E. Maruyama, S. Kuriki, Y. Kurisu, and M. Matsuda, "Analytical approach to calculate the flux dependent current-voltage characteristics of dc superconducting quantum interference devices," *Journal of Applied Physics*, vol. 83, no. 11, pp. 6166-6171, Jun 1 1998.
- [40] I. I. Soloviev, N. V. Klenov, A. E. Schegolev, S. V. Bakurskiy, and M. Y. Kupriyanov, "Analytical derivation of DC SQUID response," *Superconductor Science & Technology*, vol. 29, no. 9, Sep 2016.
- [41] T. Ryhanen, H. Seppa, and R. Cantor, "Effect of Parasitic Capacitance and Inductance on the Dynamics and Noise of Dc Superconducting Quantum Interference Devices," *Journal of Applied Physics*, vol. 71, no. 12, pp. 6150-6166, Jun 15 1992.
- [42] R. H. Ono, J. A. Koch, A. Steinbach, M. E. Huber, and M. W. Cromar, "Tightly coupled dc SQUIDs with resonance damping," *IEEE Transactions on Applied Superconductivity*, vol. 7, no. 2, pp. 2538-2541, 1997.
- [43] J. Schambach, L. Warzemann, P. Weber *et al.*, "Performance of Dc Squids with Parasitic Elements," *Superconductor Science & Technology*, vol. 7, no. 5, pp. 330-332, May 1994.
- [44] W. Wu, T. Liang, Z. Lin *et al.*, "Resonance analysis using a high frequency simulation method for dc-SQUID amplifiers," *Physica C: Superconductivity and its Applications*, vol. 591, 2021.
- [45] S. Franco, *Design with operational amplifiers and analog integrated circuits*. McGraw-Hill New York, 2002, pp. 3-50.
- [46] G. M. Gutt, J. S. Kim, M. R. Condrón, J. M. Lockhart, and B. Muhlfielder, "An ultralow noise amplifier for superconductive detectors," *Superconductor Science and Technology*, vol. 4, no. 11, pp. 633-636, 1991.
- [47] G. V. Pallottino and T. Lupi, "Low-Noise Fet Amplifier for Dc Squid," (in English), *Review of Scientific Instruments*, vol. 61, no. 9, pp. 2436-2438, Sep 1990.
- [48] N. Beev and M. Kiviranta, "Fully differential cryogenic transistor amplifier," *Cryogenics*, vol. 57, pp. 129-133, 2013.
- [49] N. Oukhanski, R. Stolz, and H. G. Meyer, "Ultra-low-drift and very fast dc SQUID readout electronics," *Journal of Physics: Conference Series*, vol. 43, pp. 1270-1273, 2006.
- [50] N. Oukhanski, R. Stolz, and H.-G. Meyer, "High slew rate, ultrastable direct-coupled readout for dc superconducting quantum interference devices," *Applied Physics Letters*, vol. 89, no. 6, 2006.
- [51] J. Zhao, Y. Zhang, Y. H. Lee, and H. J. Krause, "Investigation and optimization of low-frequency noise performance in readout electronics of dc superconducting quantum interference device," *Rev Sci Instrum*, vol. 85, no. 5, p. 054707, May 2014.
- [52] D. J. Adelerhof, J. Kawai, K. Tsukada, G. Uehara, and H. Kado, "Magnetometers Based on Double Relaxation Oscillation Superconducting Quantum Interference Devices," (in English), *Applied Physics Letters*, vol. 66, no. 17, pp. 2274-2276, Apr 24 1995.
- [53] J. M. Kim, Y. H. Lee, H. Kwon, K. Kim, and I. Sasada, "Effect of additional reference current in a reference junction-double relaxation oscillation SQUID (RJ-DROS)," (in English), *Ieee Transactions on Applied Superconductivity*, vol. 17, no. 1, pp. 13-19, Mar 2007.
- [54] D. Drung, R. Cantor, M. Peters, H. J. Scheer, and H. Koch, "Low-noise high-speed dc superconducting quantum interference device magnetometer with simplified feedback electronics," *Applied Physics Letters*, vol. 57, no. 4, pp. 406-408, 1990.

- [55] D. Drung, R. Cantor, M. Peters, T. Ryhanen, and H. Koch, "Integrated DC SQUID magnetometer with high dV/dB," *IEEE Transactions on Magnetics*, vol. 27, no. 2, pp. 3001-3004, 1991.
- [56] H. Seppä, A. Ahonen, J. Knuutila, J. Simola, and V. Volkman, "DC-SQUID electronics based on adaptive positive feedback: experiments," *IEEE Transactions on Magnetics*, vol. 27, no. 2, pp. 2488-2490, 1991.
- [57] D. Drung and H. Koch, "An integrated DC SQUID magnetometer with variable additional positive feedback," *Superconductor Science and Technology*, vol. 7, no. 5, pp. 242-245, 1994.
- [58] X. Xie, Y. Zhang, H. Wang *et al.*, "A voltage biased superconducting quantum interference device bootstrap circuit," *Superconductor Science and Technology*, vol. 23, no. 6, 2010.
- [59] R. P. Welty and J. M. Martinis, "Two-stage integrated SQUID amplifier with series array output," *IEEE Transactions on Applied Superconductivity*, vol. 3, no. 1, pp. 2605-2608, 1993.
- [60] R. Cantor, L. P. Lee, A. Matlashov, and V. Vinetskiy, "A low-noise, two-stage DC SQUID amplifier with high bandwidth and dynamic range," *IEEE Transactions on Applied Superconductivity*, vol. 7, no. 2, pp. 3033-3036, 1997.
- [61] I. Jin and F. C. Wellstood, "Continuous feedback operation of a two-stage dc SQUID system," *IEEE Transactions on Applied Superconductivity*, vol. 9, no. 2, pp. 2931-2934, 1999.
- [62] M. Podt, M. J. van Duuren, A. W. Hamster, J. Flokstra, and H. Rogalla, "Two-stage amplifier based on a double relaxation oscillation superconducting quantum interference device," *Applied Physics Letters*, vol. 75, no. 15, pp. 2316-2318, 1999.
- [63] Y. L. Wang, G. F. Zhang, S. L. Zhang *et al.*, "A Practical Two-Stage SQUID Readout Circuit Improved With Proportional Feedback Schemes," (in English), *Ieee Transactions on Applied Superconductivity*, vol. 30, no. 5, pp. 1-6, Aug 2020.
- [64] V. Foglietti, W. Gallagher, and R. Koch, "A novel modulation technique for 1/f noise reduction in dc SQUIDs," *IEEE Transactions on Magnetics*, vol. 23, no. 2, pp. 1150-1153, 1987.
- [65] D. Drung, "Improved dc SQUID read-out electronics with low 1/f noise preamplifier," *Review of Scientific Instruments*, vol. 68, no. 11, pp. 4066-4074, 1997.
- [66] H. Rogalla and C. Heiden, "A SQUID system for low-drift magnetization measurements," *Applied Physics*, vol. 14, no. 4, pp. 422-422, 1977.
- [67] N. Oukhanski, R. Stolz, V. Zakosarenko, and H. G. Meyer, "Low-drift broadband directly coupled dc SQUID read-out electronics," *Physica C: Superconductivity*, vol. 368, no. 1-4, pp. 166-170, 2002.
- [68] Y. L. Wang, S. L. Zhang, G. F. Zhang *et al.*, "Low-drift and compact readout electronics for practical SQUID magnetocardiography working in unshielded environment," (in English), *Physica C-Superconductivity and Its Applications*, vol. 575, no. 1, pp. 1-5, Aug 15 2020.
- [69] M. Hirota, T. Furuse, K. Ebana *et al.*, "Magnetic detection of a surface ship by an airborne LTS SQUID MAD," *IEEE Transactions on Applied Superconductivity*, vol. 11, no. 1, pp. 884-887, 2001.
- [70] T. Schönau, M. Schmelz, V. Zakosarenko *et al.*, "SQUID-based setup for the absolute measurement of the Earth's magnetic field," *Superconductor Science and Technology*, vol. 26, no. 3, 2013.
- [71] K. Kobayashi, M. Yoshizawa, D. Oyama, and Y. Uchikawa, "Wide Dynamic Range Analog Flux-Locked Loop System Using Low-Tc SQUID for MCG Measurements Without MSR," *IEEE Transactions on Magnetics*, vol. 50, no. 11, pp. 1-3, 2014.
- [72] M. Kiviranta and N. Beev, "Four-quadrant flux quanta counting for wide-range SQUID amplifiers," *Superconductor Science and Technology*, vol. 27, no. 7, 2014.
- [73] Y. L. Wang, G. F. Zhang, H. Dong *et al.*, "Wide Range SQUID Amplifier with Proportional Feedback for Flux Quanta Counting Scheme," (in English), *Ieee Transactions on Applied*

- Superconductivity*, vol. 30, no. 5, pp. 1-5, Aug 2020.
- [74] Y. L. Wang, G. F. Zhang, S. L. Zhang, L. L. Rong, Y. Wang, and X. M. Xie, "Two-terminal wide range SQUID amplifier with hysteretic quasi linear transfer characteristics," (in English), *Physica C-Superconductivity and Its Applications*, vol. 567, Dec 15 2019.
- [75] F. Wellstood, C. Heiden, and J. Clarke, "Integrated dc SQUID magnetometer with a high slew rate," *Review of Scientific Instruments*, vol. 55, no. 6, pp. 952-957, 1984.
- [76] S. L. Thomasson and C. M. Gould, "High Slew Rate Large Bandwidth Integrated De Squid Magnetometer for Nmr Applications," (in English), *Ieee Transactions on Applied Superconductivity*, vol. 5, no. 2, pp. 3222-3225, Jun 1995.
- [77] K. Chang, Y. Zhang, Y. Wang *et al.*, "A simple SQUID system with one operational amplifier as readout electronics," *Superconductor Science and Technology*, vol. 27, no. 11, 2014.
- [78] Y. Wang, Y. Zhang, K. Chang, H.-J. Krause, X. Xu, and Y. Qiu, "Magnetic sensor for superconducting quantum interference device using single operational amplifier," USA Patent US10551446B2, 2020.
- [79] K. Chang, L. Rong, Y. Wang, X. Kong, and X. Xie, "Two-Pole Integrator SQUID Readout Electronics With High Slew Rate and Small Closed-Loop Frequency Response Peak," *IEEE Transactions on Applied Superconductivity*, vol. 25, no. 4, pp. 1-3, 2015.
- [80] Y. L. Wang, G. F. Zhang, S. L. Zhang, L. L. Rong, Y. Wang, and X. M. Xie, "Small signal analysis of SQUID direct readout schemes," (in English), *Physica C-Superconductivity and Its Applications*, vol. 569, Feb 15 2020.
- [81] Y. L. Wang, G. F. Zhang, and S. L. Zhang, "Noise Performance Comparison Between Current- and Voltage-Bias Readout Schemes for DC SQUID," (in English), *Ieee Transactions on Applied Superconductivity*, vol. 31, no. 7, pp. 1-7, Oct 2021.
- [82] M. Schiffler, M. Queitsch, R. Stolz *et al.*, "Calibration of SQUID vector magnetometers in full tensor gradiometry systems," (in English), *Geophysical Journal International*, vol. 198, no. 2, pp. 954-964, Aug 2014.
- [83] L. Yue, D. Cheng, M. Wang, and J. Zhao, "Error Calibration for Crosstalk of SQUIDS in Full Tensor Magnetic Gradiometer Based on Moore–Penrose Inverse and Helmholtz Coil," *IEEE Transactions on Applied Superconductivity*, vol. 33, no. 3, pp. 1-10, 2023.